sustainability

MDPI

Article

Modeling, Dynamic Simulation, and Optimization of a Renewable Energy-Based Hybrid Building Energy System Incorporating Photovoltaic/Thermal Collectors, Wind Turbine, and Energy Storage: A Case Study for Antalya, Turkey

Oluwaponmile David Alao [1,*], Maaz Akhtar [2], Muhammad Abid [3], Ali Shefik [1], Mustafa Dagbasi [1], Aminu Musa Garba [4], Naser A. Alsaleh [2] and Ikenna D. Uwanuakwa [5]

[1] Department of Energy Systems Engineering, Cyprus International University, Mersin 10, Nicosia 99258, Turkey
[2] Industrial Engineering Department, College of Engineering, Imam Mohammad Ibn Saud Islamic University (IMSIU), Riyadh 11432, Saudi Arabia
[3] Department of Energy Systems Engineering, Universiti Brunei Darussalam, Jalan Tungku Link BE, Bandar Seri Begawan 1410, Brunei
[4] Civil Engineering Department, Faculty of Civil and Environmental Engineering, Near East University, Near East Boulevard, Nicosia 99138, Turkey
[5] Gordion Beton, Baskent OSB Mah. 16. Cad. No. 25 Malikoy-Sincan/Ankara, Ankara 06909, Turkey
* Correspondence: davepommyalao@gmail.com

Abstract

This paper examines the potential of solar and wind energy-based hybrid energy systems for residential applications using the meteorological data for Antalya, Turkey. To this end, a Hybrid Renewable Energy System (HRES) is designed to provide electricity, cooling, space heating, and domestic hot water to meet the energy requirements of a residential building in a remote area of Antalya. TRNSYS software is employed in the performance analysis of the system. The key findings of this study indicate that the proposed HRES is able to offer a technically dependable and economically viable energy system for residential applications through the generation of environmentally friendly and sustainable energy outputs. The HRES generated annual thermal, cooling, and electrical energy of 6916.652 kWh, 3027.083 kWh, and 2730.489 kWh, respectively. System economic analysis and optimization is also carried out to ensure the cost-effectiveness and robustness of the system. The Levelized Cost of Energy (LCOE) is found to be 0.237 USD/kWh. Multi-objective PSO optimization performed gave a CAPEX and LCOE reduction of 16.1% and 35%, respectively. This study therefore addresses the limited integrated modeling, optimization, and reliability assessment of off-grid solar–wind residential multigeneration systems under Antalya's Mediterranean climatic conditions, and it shows the potential of the HRES to save a total of 78,500 kg CO_2 emissions throughout its lifetime. These research results reveal the reliability and cost-effectiveness of the proposed renewable energy system for residential applications in Turkey.

Keywords: renewable energy; optimization; photovoltaic–thermal collectors; wind turbine; Turkey

Check for updates

Academic Editor: Marco Noro

Received: 11 August 2026
Revised: 27 October 2026
Accepted: 2 November 2026
Published: 6 November 2026

Copyright: © 2026 by the authors. Licensee MDPI, Basel, Switzerland. This article is an open access article distributed under the terms and conditions of the Creative Commons Attribution (CC BY) license.

1. Introduction

Energy is a crucial requirement in almost all aspects of everyday life. Since global warming has become a very critical issue in the world today, the source and management of energy and its production are therefore vital for sustainability, freedom from environmental

degradation, and the achievement of the United Nations Sustainable Development Goals (SDGs). Due to the increase in population and industrial production all over the world, global energy needs are also increasing at a tremendous rate. This puts the existing fossil fuels in danger of being depleted and increases greenhouse gas emissions, with the attendant environmental harm. So far, the best solution to reduce the utilization of fossil fuels, which results in a decrease in environmental pollution caused by their production and usage, is increased use of renewable energy sources. Buildings are a significant area of application for energy consumption. The supply of renewable energy for building applications, which include the provision of cooling and space heating, the supply of hot water for domestic use, and the electricity supply for household appliances and equipment, are able to reduce the consumption of fossil resources, thereby decreasing the emission of CO_2 and controlling global warming. Renewable energy sources therefore serve as effective alternatives for meeting global energy needs, which include these building energy applications. However, one of the critical challenges associated with the use of key renewable energy sources is the intermittent nature of these resources, which brings about the issue of significant performance variations. A viable solution to this issue is the provision of a hybrid renewable energy system that integrates two or more renewable energy resources to provide energy for various applications [1]. This significantly improves the system performance and reliability. Renewable energy sources such as sunlight, wind, waves, geothermal heat, and biomass can therefore be integrated to provide system reliability with improved efficiency and poly-generation capacity.

At the residential scale, the motivation for a stand-alone HRES extends beyond electricity generation to the coordinated satisfaction of the various energy services required by a building. Therefore, the integration of complementary solar and wind resources with electrical and thermal storage and appropriate conversion technologies provides a means of balancing variable renewable supply against electricity, space cooling, space heating, and domestic hot-water demands without relying on the utility grid as the principal balancing mechanism, especially for remote locations that lack access to the national electricity grid. Such integrated multigeneration configurations can also enhance the utilization of locally available renewable energy through the direction of the generated electrical and thermal energy toward diverse building demands rather than independent treatment of the services. Consequently, stand-alone residential HRESs offer a useful framework for investigating the extent to which a single building can achieve greater renewable-energy self-sufficiency while maintaining the required energy services despite temporal variations in renewable resources and demand profiles [2,3].

Within this broader context, the potential of HRESs is particularly relevant in countries and locations with abundant and complementary renewable resources. Türkiye represents an important case in this regard, given its considerable solar and wind energy potential and its ongoing transition toward a greater share of renewable energy. Turkey, a developed country and member of the Group of Twenty (G20) major economies, is blessed with a significant amount of renewable energy sources. This means renewable-based energy systems should be considered vital solutions for Turkey's sustainable development. The share of fossil fuels in Turkey's energy consumption has recorded a remarkable drop in the past few years, with the share of modern renewables in final energy consumption in the year 2022 being 13.81%. Furthermore, the renewable share of electricity generation in the country in 2022 is 42% [4]. Recent data has shown that renewable energy sources made up 45.65% of electricity generation in Turkey in the year 2024, with wind and solar power contributing a combined 18.22% and surpassing domestic coal power's historic peak in the country [5,6]. Turkey's national energy plan targets a 65% share of renewable energy in its installed overall energy capacity by 2035 [7]. With Turkey's enormous renewable energy

resources, increased research on advanced renewable energy technologies that produce renewable energy systems with enhanced performance, and favorable government policies, this target is deemed to be realizable.

Due to its geographical location, Turkey has a high energy potential, with an annual average daily solar radiation of 3.6 kWh/m^2 [8]. At the local scale, Antalya receives an average annual total solar irradiation of approximately 1600–1650 kWh/(m^2·yr), which is higher than the national average (of 1527.46 kWh/(m^2·yr) and confirms the strong solar-energy potential of the selected study location [9,10]. Antalya, which is located on the Mediterranean coast and in the southwestern part of Turkey, is one of the few Turkish metropolitan cities with a very sunny climate. The summer periods are hot and dry while the winter is generally mild. With approximately 3000 h of sunlight annually, Antalya enjoys a very sunny climate and abundant solar energy [11,12]. When it comes to wind energy potential, Turkey has favorable geographical and climatic features for wind energy. The majority of wind energy projects in Turkey are concentrated in the Mediterranean and Aegean regions. Antalya, based in the Mediterranean region, with its long coastline and presence of high-altitude mountains with intense wind conditions, therefore has sufficient potential for wind energy production. The annual average wind speed for the Mediterranean Region of Turkey ranges between 5.5 m/s and 7 m/s. The annual average wind density for the region is 21.4 W/m^2 [13–15]. Furthermore, there are remote locations in Antalya that lack access to the national electricity grid, requiring buildings to rely entirely on off-grid energy systems. While the majority of Antalya province's main municipal districts and coastal towns are fully connected to the central grids, the province's unique topography, bordered by the rugged Taurus Mountains, isolates several types of areas, making extension of the grid both physically and financially very difficult to penetrate. This situation underscores the significance of stand-alone energy systems in these remote locations. As Turkey targets an increased share of renewable energy in its installed overall energy capacity for the coming decade, this study therefore contributes to research works on renewable energy systems by presenting a multigeneration hybrid renewable energy system that is able to satisfy the energy demands of a residential building located in remote area of Antalya, Turkey. Antalya is used as the case study due to its obvious solar as well as wind resource potentials.

Numerous studies have utilized the presence of enormous or sufficient renewable energy resources in different locations of the globe to model various hybrid renewable energy systems using varied standard software that are able to carry out technical and economic analysis of the system as well as guarantee reliability and efficiency of the system. Alhijazi et al. (2023) [16] carried out a review of hybrid renewable energy systems, taking into consideration different aspects that include principles, type, sources, hybridization approach, unit energy production cost, and areas of application. In addition, the hybrid renewable energy systems with and without storage systems were considered in the review. The study observed that the popularly utilized software in the simulation, design, evaluation, and optimization of these hybridized RE systems are Greenius, HOMER, SAM, and TRNSYS. The environmental benefits of HRESs are observed from the various studies considered. The immense potential in biomass-concentrated solar energy-based HRESs was emphasized, as this integration type not only produces thermal and electrical energy alone, but it also offers solutions for environmental issues relating to waste biomass. The utilization of these hybrid renewable energy systems to produce multiple outputs increases both the environmental and economic benefits, ensuring the sustainability of the system. Various works with hybridized biomass–solar renewable energy systems revealing the benefits mentioned above can be found in the literature. Petrollese & Cocco [1] carried out an assessment of the technical and economic performance of a hybrid Concentrated Solar Power (CSP)–biogas-based system. The study developed a simulation model for the system's performance

analysis and evaluated the impacts of variation in anaerobic digester volume and the capacity of the storage tank. The system's economic analysis was carried out, and the optimal system configuration, while considering the economic aspect, was achieved with a decent biogas section that was able to supply part of the nominal input thermal energy that is needed by the power block. The efficient sizing of the biogas section leads to improved system capacity factor and efficiency. In a similar manner, El-Sattar et al. [17] presented a novel solar–biomass gasifier-based hybrid system for a rural location in Egypt. The simulation results with the optimal system sizing and improved cost using a Mayfly Optimization Algorithm (MOA) showed an energy cost of 0.2106533 $/kWh and net present cost (NPC) of $6,170,134. Godino & Garcia [18] also performed a technical and economic evaluation of a novel solar–biomass-based small-scale HRES. From the study results, the LCOE was characterized based on solar field size, biomass boilers size, and biomass consumption limitations. The finding shows that increased plant installation size has a positive impact on the LCOE, although the plant size's annual biomass consumption is expected to be compatible with the production, and in the plant's vicinity. There are also studies that employed hybridization of other renewable energy sources without inclusion of solar energy source. Bhatti et al. [19] presented a renewable energy hybrid system that combined both biomass and wind energy sources to generate electricity, cooling and space heating, fresh water, hot water, and hydrogen. The system was designed using both Simulink and Engineering Equation Solver (EES), and the results showed output power generation of 7 MW and 0.6 MW for the wind turbine section and the biogas unit, respectively.

The combination of a solar source renewable energy system and wind turbine is widely employed by researchers, and this hybridization of renewable energy sources is common in the literature as well as in real-life usage [20]. These two sources of energy complement each other as a result of varied peak production. Solar energy experiences peak periods during the day when the radiation from the Sun is intense, while wind energy often peaks in the evening or during the night when the Sun is down. When one source is less productive, the other source thus fills the gap, which ensures a constant supply of energy by the hybrid system. Afrouzi et al. [21], in their study, presented a stand-alone hybrid photovoltaic–wind system to supply electricity to a rural community in Lundu, Malaysia. The proposed system simulation was carried out using MATLAB, while the optimal sizing and cost for the hybrid PV–wind system over a 20-year period were obtained. The optimal system combination showed eleven solar panels, a wind turbine, and nine batteries with a Life Cycle Cost of RM 221,329.97 (~$54,717). Allouhi et al. [22] also proposed a solar–wind-based hybrid renewable energy system to satisfy the electrical load of a multi-family residential building with the addition of clean hydrogen production. The authors were able to substitute a Solar Dish Stirling (SDS) for conventional photovoltaic or PVT solar source to produce a SDS–Wind Turbine-based hybrid system with potential for higher efficiencies and competitive costs. The system's performance was investigated using two locations in Morocco (Quarzazate and Dakhla). The optimum system configurations from the findings indicate that Dakhla significantly favors the implementation of wind turbine technology, yielding NPC and LCOE values of 3.053 M€ and 0.0697 €/kWh respectively, while Quarzazate favors the SDS technology, yielding NPC and LCOE values of 3.391 M€ and 0.126 €/kWh, respectively. A standalone hybrid solar–wind energy system, also connected to an electrical battery system for energy storage, to electrify a single-family residential building is presented by Babalola et al. [23]. Simulation and optimization of the proposed hybrid system were performed using HOMER Pro and analyzed for three different locations in Nigeria (Kano, Anambra, and Lagos). The findings indicate that Kano shows the best economic performance indices by having a net present cost (NPC) of $32,212.52 and cost of energy (COE) of $0.6072/kWh. It was followed by Anambra

(with NPC = $45,671.68 and COE = $0.8609/kWh) and lastly Lagos (NPC = $47,184.62 and COE = $0.8706/kWh). The study thus observed that locations with higher renewable energy potential have lower energy cost. Another hybridization of a solar–wind turbines renewable system is proposed by Savio et al. [24]. The study performed the modeling and simulation of a 2.5 MW solar–wind hybrid system using MATLAB. The system was optimized for domestic grid application. The results indicate a significant reduction in the Total Harmonic Distortion (THD), with a decrease in voltage and current THD from 45.48% to 26.205 and 8.32% to 2.88%, respectively. The results therefore demonstrate the effectiveness of the proposed solar–wind-based HRES in the provision of high-quality power as well as offering sustainable energy solutions. Kumar & Majid [25] performed a feasibility study of a wind–solar hybrid energy plant, with the design strategy for the deployment of wind–solar hybrid power facilities in India examined. The study also investigated the potential challenges inherent in wind–solar hybrid technologies and proffered possible solutions to the identified challenges. While the authors design a wind–solar hybrid system for a small-scale irrigation, the study observed that large-scale hybridized wind–solar energy projects are in their early stages in India, with more research required.

Researchers have also worked on hybrid energy systems that integrate diesel generators with renewable energy sources to produce sustainable energy. He et al. [26] presented a hybrid renewable energy system with varied component combinations using HOMER software for system optimization, with Malang regency in Indonesia as the case study region. Although the case study region was connected to the grid, the study is able to show that an off-grid hybrid system consisting of PV, bio generators, diesel generators, and a battery system is able to satisfy the demand load and also provide a solution to environmental issues. A standalone hybrid system consisting of similar components, that is, solar panels, a biomass generator, a diesel generator, and a battery bank, is presented in [27] to meet the energy demands of a rural community located on an island in the Gulf of Guayaquil in Ecuador. The optimization and evaluation of the system indicate that the system's overall cost is $96,033 while the levelized cost of energy (LCOE) is $0.276/kWh, making it attractive for implementation. Ganjei et al. [28] performed the modeling and sensitivity analysis of an off-grid wind–solar-based hybrid system combined with a diesel generator and battery bank for the Turkalan rural area, located in the East Azerbaijan Province of Iran. Analysis and optimization of the proposed system was performed using HOMER software. The optimum system configuration is the solar–generator system with a battery. It gives an NPC of $3224 with a capacity of 13 kW solar panels and a 2 kW diesel generator with 17 batteries, offering a better solution to satisfy the electrical demand of the Turkalan area.

Table 1 shows an overview of some of the studies on hybrid renewable energy systems based on the literature, with key metrics such as renewable energy sources employed, location, software platform, application, energy outputs, and optimization approach provided.

Table 1. Overview of the literature review.

Ref	Year	Renewable Energy Sources	Location	Software Used	Application	Energy Outputs	Economic Metrics	Optimization Approach
[17]	2022	Solar PV and biomass	Abu-Monqar, Egypt	MATLAB	Remote area	Electricity	0.2106533 $/kWh (Energy cost)	Mayfly Optimization Algorithm (MOA)
[21]	2021	Solar PV and wind turbine	Sarawak, Malaysia	MATLAB	Rural community	Electricity	RM221,329.97 ≈ $54,717 (LCC)	LCC analysis using MARLAB code
[22]	2022	Solar Dish Stirling and wind turbine	Ouarzazate and Dakhla (Morocco)	System Advisor Model (SAM)	Residential (Multi-family buildings)	Electricity and hydrogen production	NPC/LCOE: 3.053 M€/0.0697 €/kWh (Dakhla) 3.391 M€/0.126 €/kWh (Ouarzazate)	No optimization performed
[29]	2025	Solar PV and wind turbine	Soma, Turkey	HOMER Pro and MATLAB	Rural settlement electricity supply	Electricity	$297,419 (NPC), 0.340 $/kWh (COE)	HOMER Pro
[23]	2026	Solar PV and wind turbine	Kano, Anambra, and Lagos (Nigeria)	HOMER Pro	Residential (Single-family residential building)	Electricity	NPC/COE: $32,212.52/$0.6072/kWh (Kano), $45,671.68/$0.8609/kWh (Anambra), $47,184.62/$0.8706/kWh (Lagos)	HOMER Pro
[28]	2022	Solar and wind energy	Turkalan village, East Azerbaijan province, Iran	HOMER software	Rural area electricity supply	Electricity	0.371 $/kWh (COE), $3224 (NPC)	HOMER software
[30]	2022	Solar PV and wind turbine	Northeastern region, Saudi Arabia	Mathematical models	Remote area electricity supply	Electricity	0.03883 $/kWh (minimum COE)	Crow search algorithm (CSA)
[24]	2025	Solar and wind energy	Tamil Nadu, India	MAT-LAB/Simulink	Residential (450 households)	Electricity	-	No optimization performed
[26]	2023	Solar PV and bio generator	Malang, Indonesia	HOMER software	Regional electricity supply	Electricity	0.188 $/kWh (COE), $1.02 million (NPC)	Multi-criteria decision-making (MCDM)
[31]	2022	Solar PV and wind turbine	El-Bahariya oasis, Egypt	MATLAB	HRES-sizing optimization	Electricity	COE: 21,583 $/kWh (SSA), 0.21583 $/kWh (GWO), 0.21582 $/kWh (IGWO)	SSA, GWO, and IGWO
[27]	2024	Solar and biomass	Masa 2 community, Gulf of Guayaquil, Ecuador	HOMER software	Residential (17 low-income homes)	Electricity	$0.276 (LCOE), $36,944 (TNPC)	HOMER software

Table 1. *Cont.*

Ref	Year	Renewable Energy Sources	Location	Software Used	Application	Energy Outputs	Economic Metrics	Optimization Approach
[32]	2022	Solar PV and wind turbine	Sharourah and Hafar Al-Batin (Saudi Arabia)	Mathematical models and HOMER	Electrical power generation	Electricity	NPC/LCOE: $236,571/0.33 $/kWh (Sharourah), $296,633/0.414 $/kWh (Hafar Al-Batin)	No optimization performed
[33]	2025	Solar PTC and geothermal energy	Kayseri, Turkey	Engineering Equation Solver (EES)	Hydrogen production	Electricity	0.182 $/kWh (LCOE)	No optimization performed
[34]	2023	Solar PV and wind turbine	Jarre, Ethiopia	MATLAB	Rural electrification	Electricity	0.1159 $/kWh (COE), 134,275.8 $/yr (TAC)	PSO, DE, MRFO, SFLA, RSA and RUN
[35]	2023	Solar and wind energy	Saraykoy district, Denizli province (Turkey)	HOMER software	District electrification (100-household area)	Electricity	1.61 $/kWh (unit energy cost)	HOMER software

As evident from the literature review as well as the summary in Table 1, there have been a variety of studies in the field of hybrid systems employing renewable energy sources. Additionally, several studies can be found on hybrid renewable energy systems using the climatic conditions of various cities in Turkey. However, most prior studies have centered on HRESs for residential and public buildings, focusing on electricity production only or electricity production in combination with a few other outputs using static or simplified modelling environments such as HOMER or MATLAB/Simulink. Thus, limited works focus on exploring the hybrid renewable energy resource potentials of the Mediterranean region of Turkey for multigeneration purposes. Additionally, the PVT/wind energy multigeneration system, which has many advantages that cut across both technical and economic performances, has not been widely analyzed and utilized in residential buildings under the Mediterranean climatic conditions characteristic of Antalya, Turkey. Modeling and performing dynamic simulation of this RE-based hybrid building energy system under the Mediterranean climatic conditions of Antalya significantly contributes to ongoing researches in the area of decarbonized energy in buildings as well as building energy sustainability. In summary, the main contributions of the present research are as follows:

- Modeling and dynamic analysis of a solar/wind-based hybrid building energy system to generate electricity, hot water, cooling, and space heating.
- Employing the dynamic TRNSYS 18 software as a powerful tool for the modeling and simulation of the dynamic hybrid system with a unique thermal distribution configuration and control strategy.
- Performance analysis of the proposed hybrid renewable energy system for climate-specific significance, that is, using the Mediterranean climatic condition of Antalya, Turkey.
- Optimization of system performance and provision of detailed reliability analysis across technical and economic criteria using Multi-Objective Particle Swarm Optimization (MOPSO) approach and Monte Carlo Simulation, respectively.

2. Methodology

The methodology employed for this study utilizes TRNSYS 18, SketchUp Pro 2019, and Python 3.13 environments for the design, simulation, and optimization of a hybrid renewable multigeneration energy system for a residential building under the climatic conditions of Antalya, Turkey. The HRES configuration was developed through a sequential design procedure based on building energy-service requirements, local renewable-resource availability, and component operating constraints. First, the residential electricity, cooling, space-heating, and DHW demands were established together with the Antalya meteorological conditions. PVT was selected to provide both electrical and thermal energy, while wind generation was incorporated as a complementary renewable electricity source. Because renewable production does not necessarily coincide with the building demands, battery storage was incorporated to manage electrical-energy mismatch, whereas thermal storage was used to buffer PVT heat for cooling, space heating, and DHW production. The thermal conversion components were then selected and sized according to the corresponding building loads and operating-temperature requirements, including the absorption chiller for converting PVT-derived heat into cooling. Supervisory control was subsequently implemented to coordinate energy production, storage, and distribution according to energy demands and storage/temperature constraints. The resulting configuration was dynamically simulated in TRNSYS, followed by parametric assessment of the principal design variables, model validation, economic performance analysis, and environmental assessment. System optimization is subsequently performed using Multi-Objective Particle Swarm Optimization (MOPSO). The MOPSO optimization was sequentially coupled with the TRNSYS-based

HRES model, with the technical and energy-performance outputs obtained from TRNSYS transferred to the Python optimization framework for techno-economic evaluation. An uncertainty analysis framework based on Monte Carlo Simulation was thereafter conducted to ascertain the proposed HRES's reliability. Figure 1 represents the flow chart of the methodology description, showing the dynamic modelling of the proposed hybrid energy system in TRNSYS and the system's optimization and reliability analysis conducted by applying multi-objective particle swarm optimization (MOPSO) technique and Monte Carlo simulation, respectively.

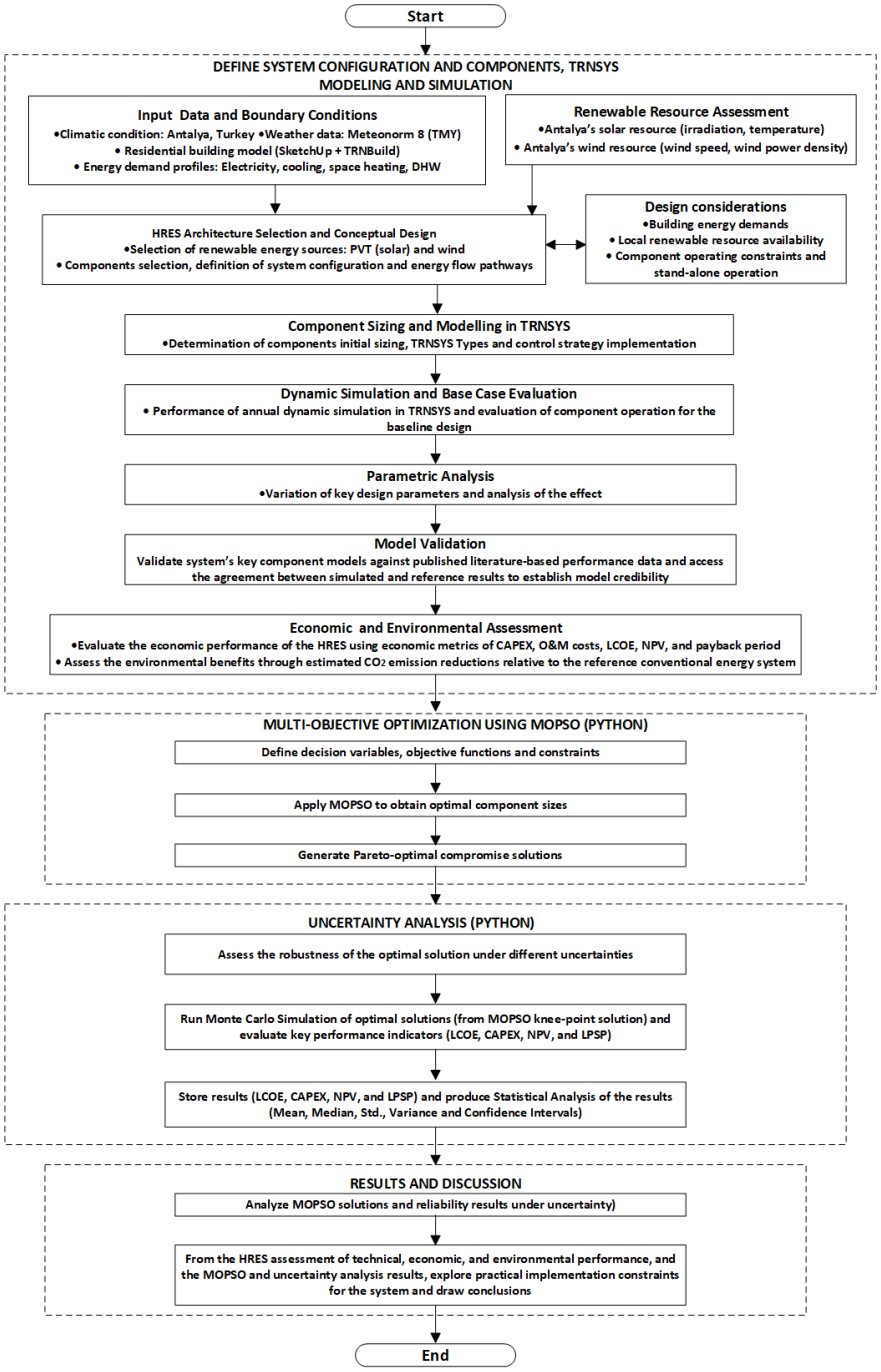


Figure 1. Flow chart showing the modelling, simulation, optimization, and uncertainty analysis of the proposed HRES.

3. Building Description and Conditioned Space

3.1. Building Description

For effective representation of the real-life system, a model of a single-family residential building with three zones was developed by utilizing SketchUp and TRNBuild. The latter is an integral part of the whole TRNSYS simulation software. The building geometry and features were first created using SketchUp. The created model was subsequently imported into TRNSYS simulation studio. The Trnsys3D plugin extension in the SketchUp environment made the file compatible with TRNSYS software. The building is oriented along the east–west axis, with its principal façade facing south. The model is divided into three thermal zones consisting of two ground-floor zones and one upper-floor zone, as shown in Figure 2. The building wall types and layers' details, as well as their u-values utilized for the building, are given in Table 2 below.

Table 2. Building construction materials.

Structure Type	Layers	Thickness (m)	Total u-Value (W/m^2K)
External wall	Finish Plaster Airspace Brick	0.01 0.09 - 0.3	0.495
Ground floor	Floor Stone Concrete Insulation	0.005 0.025 0.24 0.08	0.423
Inter-floor	Floor Stone Concrete Plaster	0.005 0.025 0.24 0.04	0.749
Inside wall	Plaster Brick Plaster Inside Film	0.013 0.23 0.02	1.314
Roof Wall	Concrete Insulation	0.20 0.16	0.258
Window	-	-	1.4

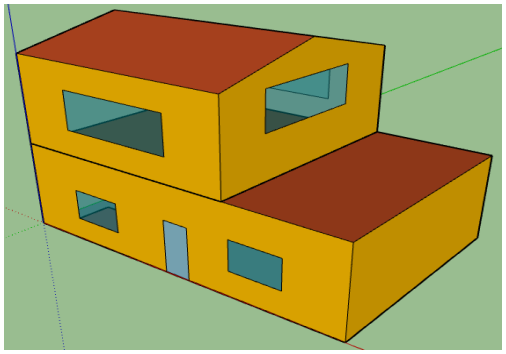


Figure 2. Building model from SketchUp.

For the determination of the U-values of the construction materials used for the building layers, the average U-values of the building elements are estimated and compared with the Turkish Standard TS 825 [36], which specifies the thermal insulation requirements for buildings. In TS 825, specifications that are less than those in the standard values are also recommended for efficiency measures. Therefore, taking into consideration the values in the

TS 825, the thermal transmittance of the construction materials for the single-story building have been selected. The external walls consist of four layers, viz., Finish, Plater, Airspace, and Brick, with their thickness shown in Table 2. The total thickness of the external wall is 0.400 m, while its thermal resistance coefficient is 0.495 W/m^{2}K. The layers that made up of other structure types in the building (inside wall, roof wall, ground floor, and inter-floor) and their thickness, as well as the total U-value, are shown in Table 2. All external windows are modeled as thermally broken aluminum-framed, argon-filled double low-e glazing units with an overall thermal transmittance of U_w = 1.40 W/m^{2}K, a solar heat-gain coefficient of g = 0.40, and visible transmittance of 0.60.

3.2. Building Conditioned Space

The instantaneous cooling load and cooling energy requirements of the modelled building are based upon heat gains (transmission) through building elements, solar radiation through windows, air exchange, and internal loads. The latter includes loads due to people, lighting, and equipment. The air exchange load includes infiltration through doors and windows and ventilation. Table 3 summarizes the key parameters used in the building conditioning design.

Table 3. Main design parameters for building conditioned space.

Parameters	Values
Set temperature for cooling	24 °C
Infiltration	Wind-speed-dependent air-change rate
Infiltration model	$ACH_{inf} = 0.07Vw + 0.4$
Lighting internal gain	2600 KJ/h
Occupant internal gain	560 KJ/h
Equipment internal gain	1000 KJ/h
Internal-gain schedule	16:00–08:00

The internal heat gains of 2600 kJ/h from lighting, 560 kJ/h from occupants, and 1000 kJ/h from electrical equipment were applied according to an internal-gain schedule from 16:00 to 08:00. The air infiltration depends on the wind velocity and was represented by the following expression:

$$ACH_{inf} = 0.07V_w + 0.4 \quad (1)$$

where V_w is the wind velocity obtained from the Antalya TMY weather file and ACH_{inf} represents the air change due to the infiltration.

4. System Description

The hybrid multigeneration renewable energy system design and simulation were carried out in the TRNSYS environment. The model architecture comprises five major loops and is presented in Figure 3. These five loops are the solar heating loop, the electrical power loop, the absorption cooling loop, the space heating loop, and the domestic hot water (DHW) production loop. The weather conditions for Antalya were represented using a Typical Meteorological Year (TMY) weather dataset generated with Meteonorm 8 and imported into TRNSYS for the annual simulation. The TMY dataset represents statistically typical long-term climatic conditions for Antalya rather than the meteorological conditions of a specific calendar year [37].

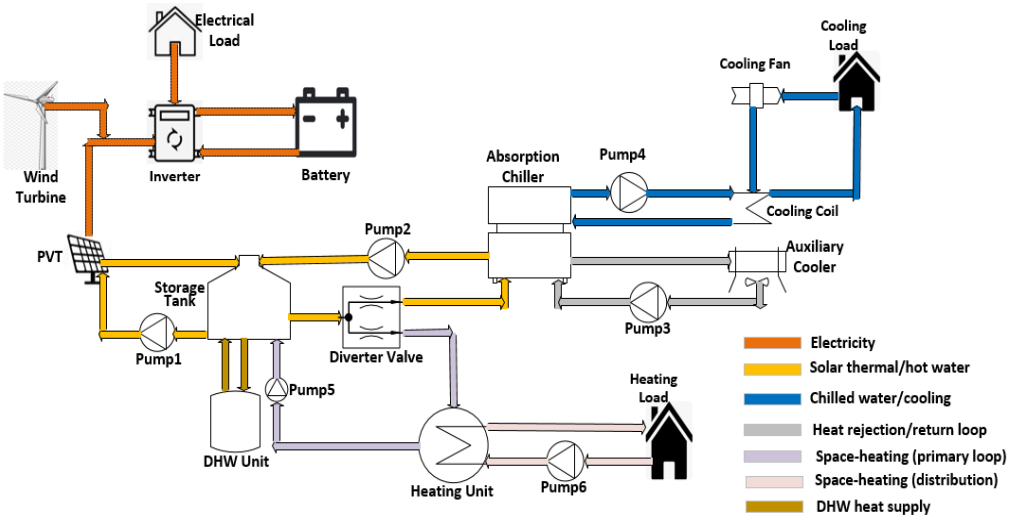


Figure 3. Schematic diagram of the proposed hybrid renewable energy multigeneration system.

The electrical load, cooling load, space heating load, and hot water consumption utilized in this study were based on a single-family residential building in Antalya, situated in the Mediterranean region of Turkey. The residential building was assumed to accommodate four occupants. The electrical-demand profile was developed using a bottom-up appliance-based approach, considering basic household appliances and their rated powers, quantities, and representative daily operating durations, as summarized in Table 4. This approach is consistent with residential load-profile studies in Türkiye, in which appliance-level electricity consumption and operating patterns are used to characterize household demand [38]. The resulting annual electrical demand of the modeled dwelling was approximately 2855.395 kWh.

Table 4. Basic appliances and electrical load data.

Equipment	Rated Power (W/unit)	Quantity	Operating Time (h/day)	Daily Electricity (kWh/day)	Annual Electricity (kWh/year)
LED lamps	18	8	5	0.720	262.800
Television	80	1	4	0.320	116.800
Refrigerator	100	1	24	2.400	876.000
Ceiling fans	75	2	5	0.750	273.750
Washing machine	1800	1	1	1.800	657.000
Laptop computer	90	1	2	0.180	65.700
Communication devices	17	3	3	0.153	55.845
Miscellaneous and auxiliary loads	—	—	—	1.500	547.500
Total	2415	17	—	7.823	2855.395

The adopted operating hours represent typical usage assumptions for the simulation, as actual appliance operating durations and consequently household electricity demand may vary according to occupant behavior, habits, appliance ownership, and usage patterns. The DHW profile was specified for the same four occupants, with a design consumption of 180 L/day at a delivery temperature of 45 °C. This design assumption follows local Antalya solar-water-heating practice that commonly sizes residential hot-water storage at roughly 40–50 L/person [39]. Additionally, some Turkish residential studies have adopted approximately similar values, as [40] reported average consumption of 45 L/day per person at 60 °C. This indicates that the present assumption, with a delivery set-point of 45 °C, provides a modest allowance for variations in occupant hot-water-use behavior.

4.1. Solar Heating Loop

The major components of the solar heating loop in the proposed system are the PVT collectors, the storage tank, and a pumping system that delivers heated fluid to the storage tank. The Antalya weather data component (TRNSYS type15) also belongs to this unit. The PVT system has eleven PVT panels, each having a rated power of 275 W. The electrical characteristics of the collectors are obtained from "Wiosun C275M" solar panels, manufactured by the German company "Wiosun". Each solar collector module has a surface area of 1.46 m^2, comprising of 60 monocrystalline cells, each having a size of 156 mm × 156 mm. The efficiency of the solar cells used in the module is 16.9% [41]. For the thermal characteristics of the PVT collectors, the parameters employed in the TRNSYS component for the PVT collector (Type 50b) are shown under Table 3. The PVT collectors are connected to a regulator–battery system as shown in Figure 2. The solar energy not utilized for electricity production is converted into thermal energy, which heats the working fluid that flows into the main storage tank with a capacity et of 2 m^3. The main thermal storage capacity provides adequate short-term buffering between the intermittent PVT thermal supply and the thermal loads while avoiding excessive storage volume and thermal inertia.

4.2. Electrical Power Loop

The generated electrical power from the system's PVT collectors is sent into a regulator–battery unit, that consists of an inverter and a set of two batteries (each 250 Ah and 24 V) connected in series to store the surplus or unused electrical energy generated and enable its further use as the need arises. The wind turbine unit also falls under the electrical power loop. The wind turbine data are obtained from the YWS-500 Wind Luce specification data for the YWS 500W-rated power capacity wind turbine at a wind speed of 12.5 m/s [42].

The electric load comprises the electrical power required by some components of the system loops, such as the pumps, and the electrical power demand of the single-family residential building being considered in this study. Surplus electricity generated is stored in the batteries while the regulator controls the battery charge and discharge operation. The daily electricity demand for a typical single-family residential building that consists of basic lighting and electrical equipment for a lower/middle-income family in Turkey is generated [43]. Figure 4 shows the monthly electricity demand for a single-family residential building as implemented in the TRNSYS simulation. The average monthly electrical load for the building is 237.95 kWh.

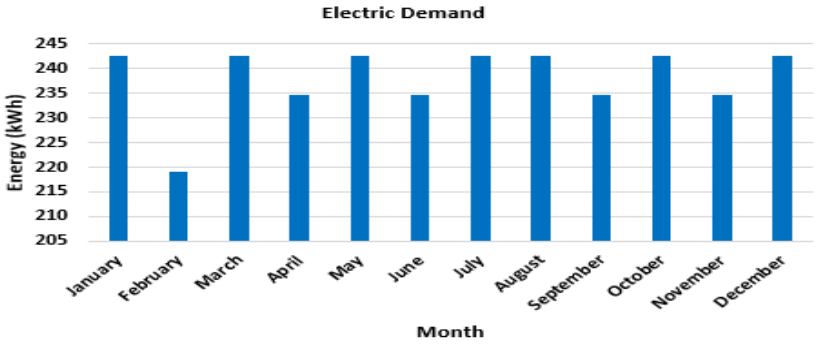


Figure 4. Monthly electricity demand for a single-family residential building.

4.3. Absorption Cooling Loop

The absorption cooling loop is part of the thermal comfort unit and consists of the absorption chiller, cooling coil, cooling fan, auxiliary cooler (condenser), and the pumping system within the loop. The required thermal energy for the operation of this loop is

transferred to the absorption chiller by the supply of hot water through the main storage tank at 75 °C. The hot water received by the absorption chiller is employed to evaporate the refrigerant and, subsequently, the absorption chiller supplies chilled water to the air-cooling coil represented by Type 32 in TRNSYS. A single-speed fan (Type 112) circulates the room air through the cooling coil. The household cooling load generated from TRNSBuild is supplied by the absorption system through the flow stream loads model (standard component Type 682 in TRNSYS) in combination with the cooling load data reader. The monthly cooling demand generated from the residential building using Antalya climatic conditions is shown in Figure 5. The total annual cooling demand for the single-family residential building is 2842.01 kWh. The occupancy schedule in a working day, with a maximum of four people considered to live in the building, is from 4:00 p.m. to 8:00 a.m.

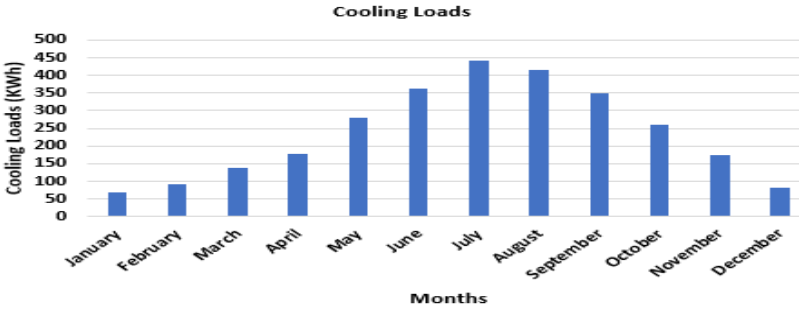


Figure 5. Building monthly cooling demand.

The absorption chiller utilized for this study is component Type 107 in TRNSYS, which is a hot water-fired single-effect absorption chiller. The absorption chiller sizing was realized based on the maximum hourly cooling load obtained from TRNSYS simulation. The peak cooling load was 9.47 kW; therefore, applying a 15% design margin gives 9.47 × 1.15 = 10.89 kW. Accordingly, a nominal 11 kW single-effect LiBr-H_2O absorption chiller was adopted, providing an actual capacity margin of approximately 16.2% above the simulated peak cooling load. The specifications of the adopted 11 kW model are based on the residential-scale 11 kW LiBr-H_2O absorption system reported by Florides et al. [44].

The hot water stream serves as the input energy to the chiller's generator. The equation guiding the imposition of the generated cooling loads onto the chilled water stream is expressed as

$$Q_{coolingload} = \dot{m_{chw}} C_p (T_{in} - T_{out}) \quad (2)$$

where C_p is the specific heat capacity of water (4.19 kJ/kg·K), $\dot{m}_{chw}$ represents the chilled water mass flow rate, and T_{in} and T_{out} are the chilled water inlet and outlet temperatures.

4.4. Space Heating Loop

The space heating loop consists of the heat exchanger, two pumping systems, the flow diverter, the flow mixer, and a controller. The diverting valve from the solar heating unit coordinates with the heat exchanger in the space heating loop, as well as the absorption chiller in the absorption cooling loop, in order to operate both units and achieve thermal comfort for the building as demanded. The heating loads generated for the residential building located in Antalya, Turkey come in the winter months of December, January, and February and amount to a total of 146.030 kWh.

4.5. Domestic Water Heating Loop

The domestic hot water (DHW) heating loop consists of the domestic hot water tank and variable pump, flow diverter, flow mixer, and a differential controller. The DHW tank's capacity is 0.5 m^3. The delivery set point temperature is 45 °C. The modeling of

the domestic water heating loop with the constituent components has been configured to achieve this set point temperature for domestic applications. A tempering valve, which is a temperature-controlled flow diverter, adjusts the output temperature of the hot water tank to a set point temperature.

It is subsequently connected to a tee-piece flow mixer. The latter carries out the mixing of the higher temperature stream that emanates from the hot water tank and the low-temperature stream from the city water mains. This ensures the achievement of the set steady temperature of 45 °C for household applications. The operation of the variable speed pump is controlled by the differential controller within the loop and aids in the recirculation of the hot water within the loop. Figure 6 depicts the total daily consumption of hot water for a single-family residential building as designed for this study in TRNSYS. The daily hot water load profile is 180 L per day.

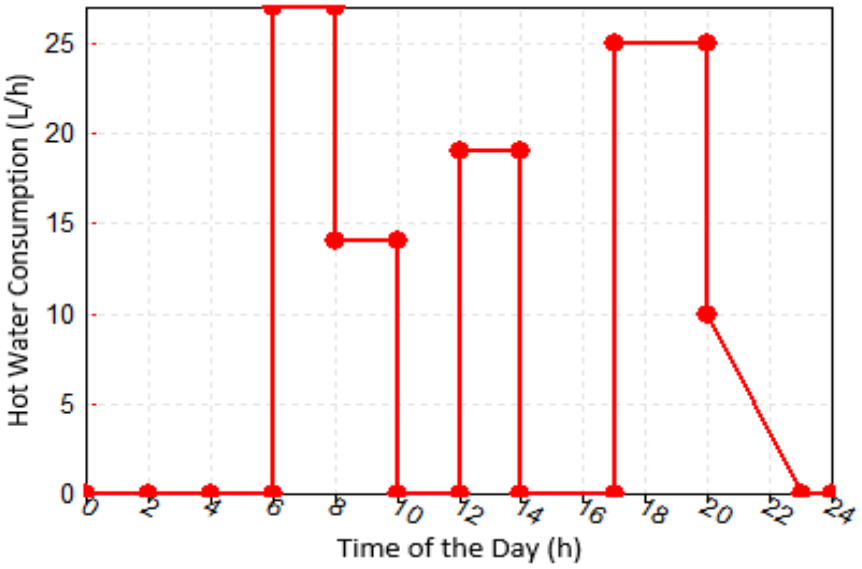


Figure 6. Daily hot water load profile designed for a single-family residential building (180 L/day).

The five major loops in the proposed HRES as modeled in TRNSYS are presented in Figure 7. The major components and their parameters employed in the system modelling are shown in Table 5, while all equipment and their respective types in TRNSYS used in the simulation are presented in Table 6.

Table 5. The main components and parameters of the system.

Component	Parameter	Value
PVT collectors	Number of pieces	11
	Area	16.0 m^2
	Collector fin efficiency factor	0.96
	Collector plate absorptance	0.90
	Collector plate emittance	0.09
	Loss coefficient for bottom and edge losses	1.1 kJ/(h.m^2·K)
	Collector slope	38°
	Temperature coefficient of PV cell	0.0032 k^{-1}
	Nominal temperature for cell	25 °C
	Cell efficiency at reference conditions	16.9%

Table 5. *Cont.*

Component	Parameter	Value
Wind Turbine	Rated Power	500 W
	Rated wind speed	12.5 m/s
	Rotor Diameter	1.558 m
	Turbine weight	17.5 kg
	Start-up wind speed	1.0 m/s
	Cut-in wind speed	1.5 m/s
	Charging wind speed	2.5 m/s
	Survival Wind Speed	60 m/s
	Number of Blades	3
Absorption chiller	Cooling capacity	11.0 kW
	Coefficient of performance	0.74
	Heat input to the generator	14.9 kW
	Absorber heat, rejected to the environment	14.1 kW
	Condenser heat, rejected to the environment	11.8 kW
	Evaporator output power	11.0 kW
Thermal storage tank	Tank type	Stratified
	Tank loss coefficient	0.8 W/(m^2·K)
	No. of nodes	10
Battery	Type	Lead-acid
	Quantity	2 pieces
	Unit voltage	24 VDC
	Unit capacity	250 Ah
	Minimum SOC	30%
	Maximum SOC	100%
	Charging efficiency	0.85
Heat exchanger	Heat exchanger effectiveness	0.65
	Specific heat of source side fluid	4.19 kJ/(kg·K)
	Specific heat of load side fluid	4.19 kJ/(kg·K)

Table 6. Equipment and Types simulated in TRNSYS.

Item	Type
Weather data	15
PVTs	50b
Wind turbine	90
Battery	47a
Inverter	48b
Electric demand	14h and 41c
Storage tank	4a
Absorption chiller	107
Cooling coil	32
Auxiliary cooler	92
Cooling fan	112b
Imposed loads	682
Data reader	9c
Pumps	3d
Variable speed pump	110
Heat exchanger	91
Controller	165b
Diverter	11b
Flow mixer	11h
City mains	14b

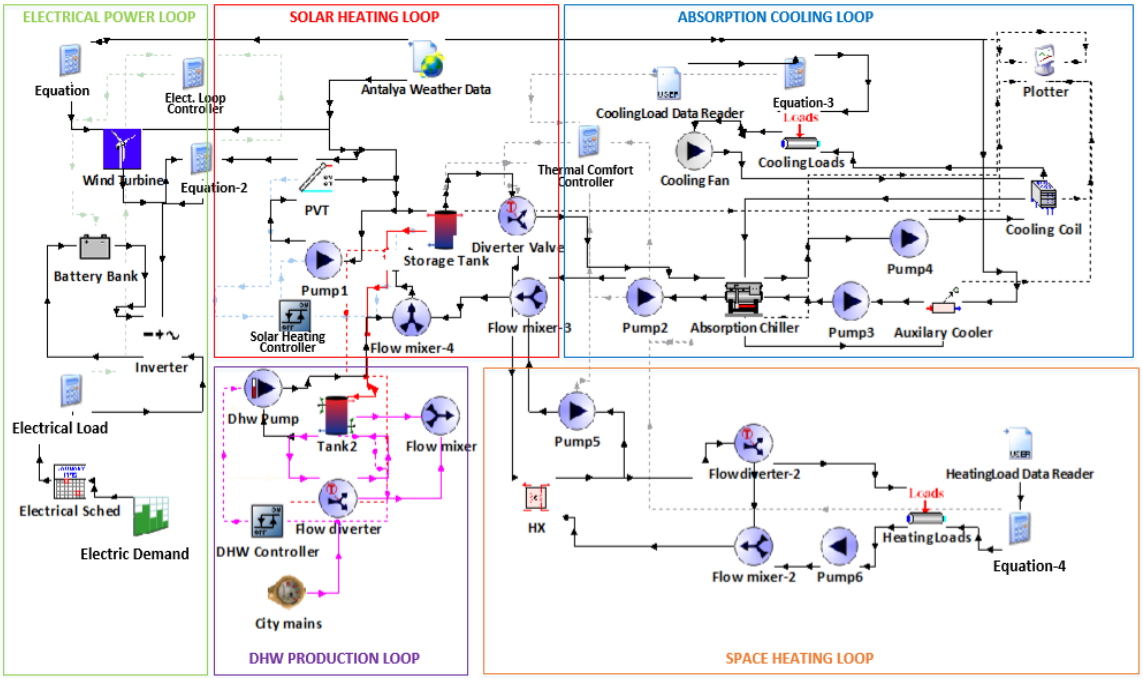


Figure 7. Simulation of the proposed hybrid RE multigeneration system, designed in TRNSYS.

4.6. Control Strategy

The control mechanism employed in the modelling of the proposed HRES comprises four control strategies, each one for each loop within the system, with the exception of the absorption cooling and space heating loops, which have a joint control strategy. These four control strategies are all implemented within the TRNSYS environment, utilizing differential controllers, built-in equation components, load-data readers, and flow diversion and mixing components. The description of these control strategies is provided in this section, with the corresponding control flowcharts for the four strategies illustrated in Figure 8.

The electrical power loop controller is responsible for electrical energy management. It monitors the renewable electrical production from both PVT and wind turbine. The electrical production is defined as $P_{RE} = P_{PVT,el} + P_{WT}$, with direct supply of the residential load (P_L) given first priority. When $P_{RE} > P_L$, surplus renewable electricity charges the battery, provided the state of charge (SOC) < 1.00; when $P_{RE} < P_L$, the battery supplies the deficit, provided SOC > 0.30. The battery operates within a state of charge interval of 30 to 100%. A charging efficiency of 0.85 is applied to the battery model. The battery discharge is represented by the TRNSYS Type 47a model formulation, and this includes the electrical losses associated with its internal battery characteristics. The solar heating loop controller receives input from the PVT modules and the main storage tank. The heat transfer from the PVT array to the main thermal storage is governed by a differential-temperature controller. The controlled temperature difference is $\Delta T = Tpvt,out - Ttank,top$. An upper deadband of $\Delta T_H = 10$ °C and lower deadband of $\Delta T_L = 2$ °C were adopted. Accordingly, the controller makes a comparison between the PVT modules outlet temperature and the temperature of the top of the main storage tank, so that pump 1 is switched ON when $\Delta T \geq 10$ °C and it is switched OFF when $\Delta T \leq 2$ °C. The hysteresis between the ON and OFF thresholds prevents rapid pump cycling when the two temperatures approach one another.

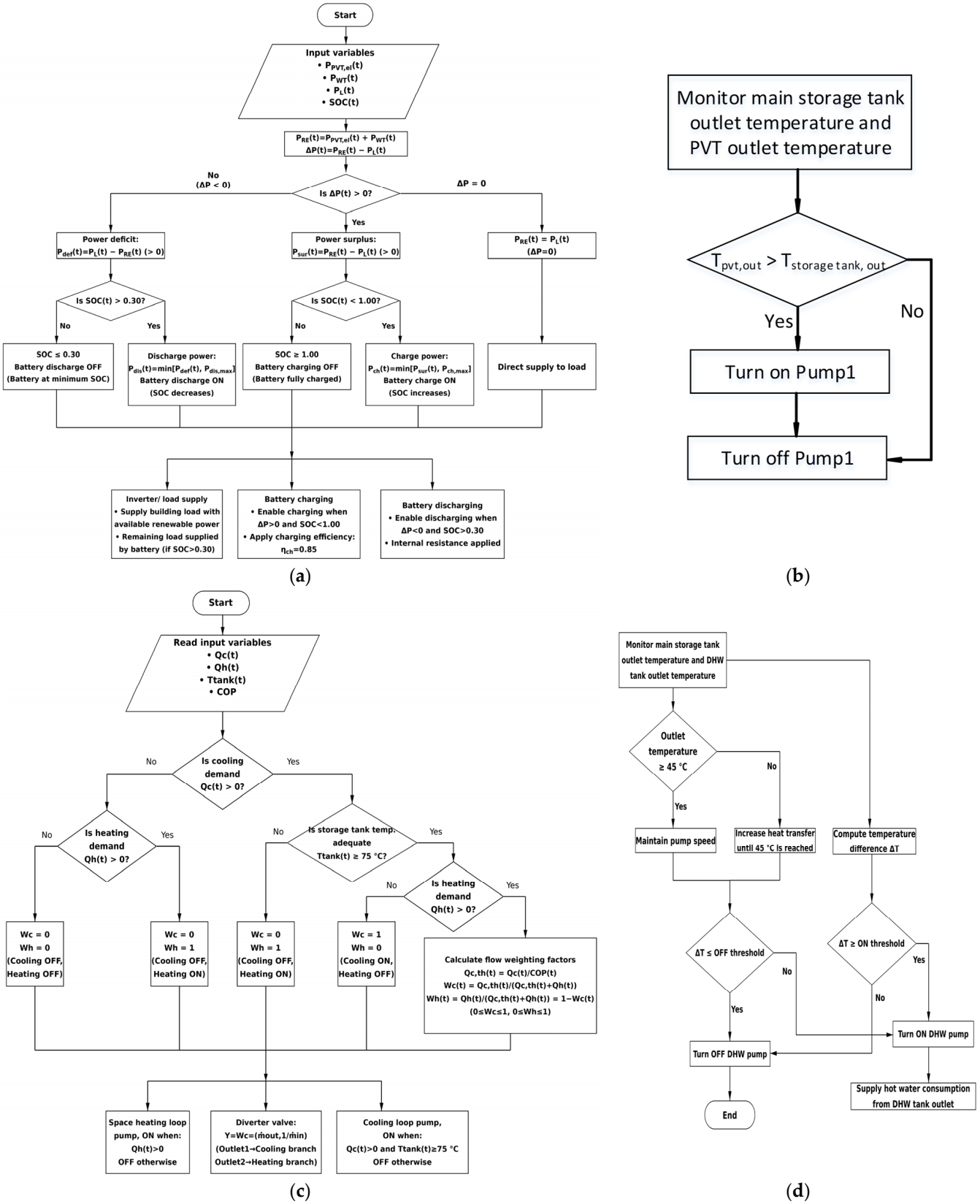


Figure 8. Flowcharts of the four control mechanisms utilized for the loops in the proposed HRES: (**a**) Electrical power loop controller; (**b**) solar heating loop controller; (**c**) absorption cooling and space heating loops controller; (**d**) domestic hot water production loop controller.

Since the building cooling loads and space heating loads depend on the atmospheric conditions, it is possible to run both the absorption cooling loop and the space heating loop using a diverter valve. The control scheme for these space comfort loops therefore considers the building cooling and space heating loops. The thermal-comfort controller therefore receives the cooling load *Qc* and the space-heating load *Qh* from their respective TRNSYS load-data readers. A positive load (Q > 0) constitutes an active demand request. Because the cooling demand represents useful cooling output, whereas the storage tank supplies generator heat to the absorption chiller, the cooling demand is converted to its generator-side thermal requirement according to $Q_{c,th} = Q_c/COP$. The cooling branch is enabled only when $Qc > 0$ and the required generator-temperature operating range of 75–95 °C is satisfied. Four thermal-comfort operating states are implemented. When $Qc = Qh = 0$, both comfort branches remain inactive. When $Qc > 0$, $Qh = 0$, and the generator-temperature criterion is satisfied, the available comfort-loop thermal flow is directed to the absorption chiller. Conversely, when $Qc = 0$ and $Qh > 0$, the available useful thermal flow is directed to the space-heating branch. When cooling and heating demands occur simultaneously and the absorption-chiller temperature criterion is satisfied, the available hot-water flow is distributed according to the instantaneous thermal requirements. The defined cooling and heating weighting factors are $w_c = Q_{c,th}/Q_{c,th} + Q_h$ and $w_h = Q_h/Q_{c,th} + Q_h$, where $w_c + w_h = 1$. The corresponding mass-flow rates are $\dot{m}_c = w_c\dot{m}_{avail}$ and $\dot{m}_h = w_h\dot{m}_{avail}$. These equations were implemented using a TRNSYS Equation component connected to the flow-diverter valve, with the function defined as $Y = \dot{m}_{out,1}/\dot{m}_{in}$. Outlet 1 is assigned to the absorption cooling loop, imposing $Y = w_c$, while the complementary fraction $1 - Y = w_h$ is channeled to the space-heating loop. This joint control mechanism for the absorption chiller loop and space heating loop making use of diverter valve helps in prioritizing the required loop for the thermal energy based on real-time building demands. The control strategy employed at the domestic hot water production loop uses a temperature differential controller (TRNSYS Type165b) alongside tempering valve (a flow diverter—Type11b in TRNSYS) and tee-piece (a flow mixer—Type11h in TRNSYS) in order to achieve a hot water delivery-set point temperature of 45 °C for domestic purposes. A detailed description of this configuration has been provided under Section 4.5. The differential controller in the DHW production loop therefore controls the DHW variable pump located between the main storage tank and the DHW tank in recirculating the heated water back into the main tank. With this arrangement, the heat transfer is modulated to sustain a stable 45 °C supply. The flowcharts of the four control strategies utilized for the loops in the proposed HRES are depicted in Figure 8.

5. Dynamic Modelling and Analysis

The assumptions considered in the system modelling and the energy and exergy analysis of the system are presented in this section. The dynamic simulation of the proposed system has been carried out in TRNSYS software. The energy, exergy, and economic analysis of the system have therefore been carried out. This makes it possible to examine the impacts of the major system components and their variables on system performance.

5.1. Assumptions

In the modelling process, for simplification of the thermodynamic simulation of the proposed hybrid renewable energy system, some appropriate assumptions are considered. The constraints and assumptions considered throughout this study are therefore presented here:

- The thermal properties and optical performance of the different PVT layers, as well as all thermal components within the system, have been assumed to remain unchanged since their performance hardly varies within the operating conditions [45,46].
- Heat transfer property changes or phase changes of all components is considered to be negligible [47,48].
- The hot water storage tank is fully layered [45].
- Except for the use of pumps and flow diverters, pressure fluctuations in the piping system of the hybrid RES are neglected [49].
- In the case of the wind turbine unit, the wind flow is considered to be uni-dimensional and incompressible [48].

5.2. Energy Analysis

The energy analysis of the hybrid renewable energy system components has been performed under dynamic operating conditions using the time-varying ambient conditions provided by Antalya TMY weather data. An adopted reference temperature of 20 °C is used in the analytical thermodynamic formulation and should not be interpreted as a constant ambient temperature imposed throughout the annual TRNSYS simulation. The governing mathematical expressions, based on the first law of thermodynamics, are provided in this section. The schematic diagram in Figure 9 shows the system components considered for the analysis. The energy balance equation can be written as given below [45].

$$\dot{Q} - \dot{W} = \sum \dot{m}_{out} h_{out} - \sum \dot{m}_{in} h_{in} \quad (3)$$

where Q and W represent the rate of thermal energy and the rate of work done, respectively.

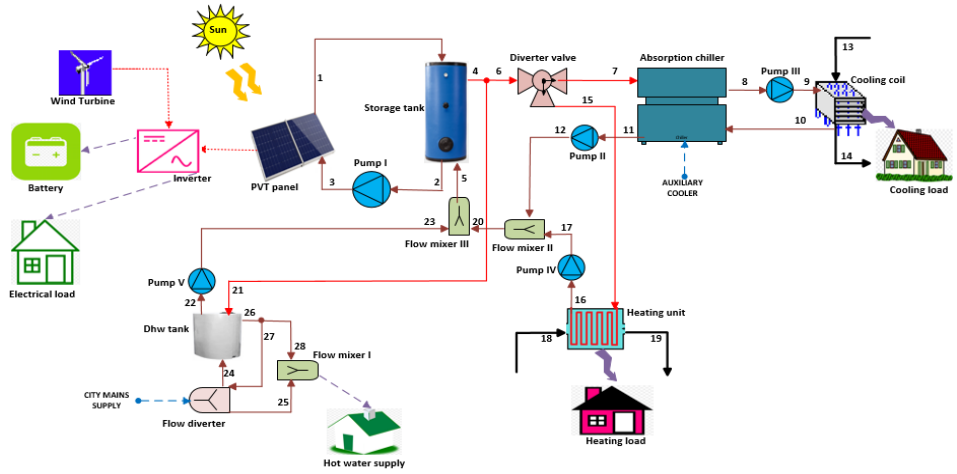


Figure 9. Schematic diagram of the proposed HRES for the first and second laws of thermodynamics analysis.

5.2.1. Wind Turbine Unit

Wind energy is a type of kinetic energy due to an air mass m flowing at a speed V. In carrying out the energy analysis of a wind turbine system, the air mass flow's kinetic energy is given as

$$E = \frac{1}{2} m V^2 \quad (4)$$

where m is mass and V is velocity. This may be expressed as given in Equation (5), [50]:

$$E = \frac{1}{2} \rho A t V^3 \quad (5)$$

where ρ is density of air, A is rotor swept area, and t is the time interval considered. Given that the flow of air mass to the wind turbine rotor per unit time is $\dot{m}$, application of the basic momentum theory gives the rate of change in momentum to be equal to the product of overall velocity change and the mass flow rate $\dot{m}$, as expressed below:

$$\dot{M} = \dot{m}(V_1 - V_2) \tag{6}$$

where V_1 and V_2 stand for the upwind and downwind speeds respectively. The power absorbed by the wind turbine can therefore be expressed as [51]:

$$P = \dot{m}(V_1 - V_2)V_{avg} \tag{7}$$

where *Vavg* is the average flow speed at the wind turbine rotor and equals to $(V_1 + V_2)/2$. The rate of kinetic energy change of the wind flow is expressed as

$$\dot{E} = \frac{1}{2}\dot{m}\left({V_1}^2 - {V_2}^2\right) \tag{8}$$

according to the energy conservation theory, Equations (7) and (8) are equal and therefore result in

$$V_{avg} = \frac{1}{2}(V_1 + V_2) \tag{9a}$$

$$V_1 - V_{avg} = V_{avg} - V_2 \tag{9b}$$

it is considered that the direction of the wind flow to the turbine hub is axial with a uniform flow velocity. Subsequently, the rotor power can be calculated as

$$P = \rho A(V_1 - V_2)V_{avg}^2 \tag{10}$$

Equation (9) can be further reduced to [52]

$$P = \frac{\rho A V_1^3}{4}\left[(1 + \alpha)\left(1 - \alpha^2\right)\right] \tag{11a}$$

$$P = \frac{\rho A V_1^3}{4}C_p \tag{11b}$$

where $\alpha = V_2/V_1$ and $C_P = (1 + \alpha)(1 - \alpha^2)$. The wind-power expression incorporates the conventional kinetic energy factor of 0.5, while *Cp* denotes the dimensionless rotor power coefficient, defined as the ratio of extracted mechanical power to the available wind power, which is

$$C_p = \frac{P_{WT}}{0.5\rho A V_1^3} = \frac{2P_{WT}}{\rho A V_1^3} \tag{11c}$$

From differentiation, it is obvious that the power P will attain the maximum value when $\alpha = \frac{1}{3}$, that is, when the final wind velocity V_2 is equal to one third of the upwind velocity V_1. Therefore, under the axial-flow conditions, the theoretical maximum power coefficient is obtained as $C_{P_{max}} = \frac{16}{27} \approx 0.593$ and is referred to as the Lanchester–Betz limit [53]. It represents the ideal Betz limit. The energy efficiency for the wind turbine is expressed as [54,55]

$$\eta = \frac{W_{out}}{E_{wind,in}} \tag{12}$$

where W_{out} represents the useful work output and $E_{wind,in}$ is the overall energy input.

5.2.2. Solar PVT Unit

By considering the first law of thermodynamics, the expression for energy balance of a PVT system can be written as [56]

$$\sum \dot{E}_{in} = \sum \dot{E}_{loss} + \sum \dot{E}_{out} \tag{13}$$

where $\dot{E}_{in}$ and $\dot{E}_{out}$ represent the input and output energy rates, respectively, and $\dot{E}_{loss}$ represents the rate of energy losses, which is given in Equation (14) as

$$\sum \dot{E}_{loss} = \dot{Q}_{loss,rad} + \dot{Q}_{loss,conv} + \dot{Q}_{loss,friction} \tag{14}$$

where $\dot{Q}_{loss,rad}$ and $\dot{Q}_{loss,conv}$ are heat loss rate by radiation and convection, respectively, and $\dot{Q}_{loss,friction}$ is energy loss due to friction. Equation (14) can therefore be expressed as

$$\dot{E}_{mass,in} + \dot{E}_{sol} = \sum \dot{E}_{loss} + \dot{E}_{elect} + \dot{E}_{mass,out} \tag{15}$$

where $\dot{E}_{sol}$ is the incident solar radiation expressed as the product of the glass cover transmissivity (τ), the cell absorptivity (α), and solar radiation flux ($\dot{G}$), as shown in Equation (16).

$$\dot{E}_{sol} = \dot{G}_{eff} = \tau \times \alpha \times \dot{G} \tag{16}$$

where $\dot{G}_{eff}$ is the effective solar irradiation in Watts. The useful heat energy transfer rate for a PVT system is the heat absorbed by the cooling fluid from the PVT collector and can be obtained from Equation (16) below:

$$\dot{E}_{th} = \dot{E}_{mass,out} - \dot{E}_{mass,in} = \dot{m}c_p\left(T_{f,out} - T_{f,in}\right) \tag{17}$$

where $\dot{m}$, c_p, and $(T_{f,out} - T_{f,in})$ represent the cooling fluid mass flow rate, specific heat capacity, and the cooling fluid temperature difference. Therefore, Equation (16) gives

$$\dot{E}_{th} = \dot{m}_3 c_p (T_1 - T_3) \tag{18}$$

The rate of electrical energy produced by solar PVT panels is given by [56]

$$\dot{E}_{elect} = V_{oc} I_{sc} F \tag{19}$$

where V_{oc}, I_{sc}, and F represent the open circuit voltage, the short circuit current, and the PV panel's fill factor under standard test conditions. The total power of the PVT panel is therefore expressed as

$$\dot{E}_{total} = \dot{E}_{th} + \dot{E}_{elect} \tag{20}$$

Since a PVT collector has both thermal and electrical efficiencies, both efficiencies are given by Equation (21) and Equation (22), respectively, as [56]

$$\eta_{th} = \frac{\dot{E}_{th}}{\dot{E}_{sol}} = \frac{\dot{E}_{mass,out} - \dot{E}_{mass,in}}{\dot{E}_{sol}} \tag{21}$$

$$\eta_{elect} = \frac{\dot{E}_{elect}}{\dot{E}_{sol}} = \frac{V_{oc} I_{sc} F}{\tau \times \alpha \times \dot{G}} \tag{22}$$

5.2.3. Absorption, DHW, and Cooling Unit

Based on the formulation of the energy balance for different parts of the proposed HRES using Equation (3) given above, the energy balance equations for the components of the absorption, DHW, and cooling units are expressed in this section. The summary of these energy relations for the proposed system's components is shown in Table 7.

Table 7. Energy balances for the various components of the proposed HRES.

Component	Energy Balance Equation
Pump I	$\dot{W}_{PI} = \dot{m}_2(h_2 - h_3)$
Pump II	$\dot{W}_{PII} = \dot{m}_{11}(h_{11} - h_{12})$
Pump III	$\dot{W}_{PIII} = \dot{m}_9(h_8 - h_9)$
Pump IV	$\dot{W}_{PIV} = \dot{m}_{16}(h_{16} - h_{17})$
Pump V	$\dot{W}_{PV} = \dot{m}_{22}(h_{22} - h_{23})$
Storage tank	$\dot{W}_{St.Tank} = \dot{m}_1h_1 + \dot{m}_5h_5 - \dot{m}_2h_2 - \dot{m}_4h_4$
Absorption chiller	$\dot{Q}_{Chill} = \dot{m}_7(h_7 - h_8) = \dot{m}_{10}(h_{11} - h_{10})$
Cooling coil	$\dot{Q}_{C.Coil} = \dot{m}_9(h_9 - h_{10}) = \dot{m}_{12}(h_{12} - h_{13})$
DHW tank	$\dot{W}_{Dhw.Tank} = \dot{m}_{21}h_{21} + \dot{m}_{24}h_{24} - \dot{m}_{22}h_{22} - \dot{m}_{26}h_{26}$
Flow diverter	$\dot{Q}_{Mains.supply} = \dot{m}_{24}h_{24} + \dot{m}_{25}h_{25} - \dot{m}_{27}h_{27}$
Flow mixer I	$\dot{Q}_{Dhw.out} = \dot{m}_{25}h_{25} + \dot{m}_{28}h_{28}$
Flow mixer II	$\dot{m}_{20}h_{20} = \dot{m}_{12}h_{12} + \dot{m}_{17}h_{17}$
Flow mixer III	$\dot{m}_5h_5 = \dot{m}_{20}h_{20} + \dot{m}_{23}h_{23}$
Heating unit	$\dot{Q}_{Heat.unit} = \dot{m}_{15}(h_{15} - h_{16}) = \dot{m}_{18}(h_{18} - h_{19})$
Diverter valve	$\dot{m}_6h_6 = \dot{m}_7h_7 + \dot{m}_{15}h_{15}$

5.3. Exergy Analysis

The exergy of a system represents the maximum amount of useful work that can be obtained from the system when in equilibrium with its surroundings. According to the second law of thermodynamics, exergy analysis represents an alternative useful tool in the design and analysis of various energy systems, which include both renewable and conventional energy systems as well as hybrid systems. In carrying out the exergy analysis for a system, the exergy balance equation for a component can be written as [57]

$$\dot{E}_F = \dot{E}_P + \dot{E}_L + \dot{E}_D \tag{23}$$

where $\dot{E}_F$, $\dot{E}_P$, $\dot{E}_L$, and $\dot{E}_D$ represent the fuel exergy rate, product exergy rate, exergy loss rate, and the rate of exergy destruction, respectively. The general exergy balance can also be expressed as [58]

$$\sum \dot{E}x_{in} - \sum \dot{E}x_{out} = \sum \dot{E}x_D \tag{24}$$

This can be expanded to give

$$\dot{E}x_Q - \dot{E}x_W + \dot{E}x_{mass,in} - \dot{E}x_{mass,out} = \dot{E}x_D \tag{25}$$

Since the exergy rate can be expressed as

$$\dot{E} = \dot{m}e \tag{26}$$

where $\dot{m}$ represents mass flow rate and e is the exergy, the exergy balance can therefore finally be expressed as [59]

$$\dot{E}x_Q - \dot{E}x_W = \sum \dot{m}_{out}e_{out} - \sum \dot{m}_{in}e_{in} + \dot{E}x_D \tag{27}$$

where $\dot{E}x_Q$, $\dot{E}x_W$, and $\dot{E}x_D$ represent the thermal exergy, work exergy, and the exergy destruction, respectively.

5.3.1. Wind Turbine Unit

Since the total exergy of a flow with unit mass usually consists of the potential, kinetic, chemical, and physical parts, in carrying out the exergy analysis of a wind turbine system, both the potential and chemical exergies are negligible. Therefore, the total exergy for a wind turbine is reduced to the sum of the kinetic exergy and the physical exergy components and is expressed as

$$\dot{E}x = \dot{E}x_{ke} + \dot{E}x_{ph} \tag{28}$$

For negligible potential energy change and negligible inlet physical/chemical exergy relative to the ambient state, the incoming wind exergy is essentially its kinetic energy rate and is expressed in Equation (29) as

$$\dot{E}x_{wind,in} = \frac{1}{2}\dot{m}V_1^2 \tag{29}$$

Additionally, the useful turbine exergy output is the electrical power, so that

$$\dot{E}x_{WT,out} = \dot{W}_{elect} \tag{30}$$

Hence,

$$\dot{E}x_D = \dot{E}x_{wind,in} - \dot{W}_{elect} - \dot{E}x_{wind,out} \tag{31}$$

where explicitly considering the residual downstream kinetic energy gives

$$\dot{E}x_{wind,out} = \frac{1}{2}\dot{m}V_2^2 \tag{32}$$

The exergy efficiency can consequently be expressed as [54,55]

$$\eta_{ex,WT} = \frac{\dot{W}_{elect}}{\dot{E}x_{wind,in}} = \frac{W_{out}}{Ex_{in}} \tag{33}$$

where the electrical power ($\dot{W}_{elect}$) represents the useful work output, and the available incoming wind kinetic exergy is treated as the exergy input.

5.3.2. Solar PVT Unit

The exergy balance for a PVT collector is generally expressed as [60]

$$\sum \dot{E}x_{in} - \sum \dot{E}x_{loss} = \sum \dot{E}x_{out} \tag{34}$$

Equation (34) can therefore be expressed as

$$\dot{E}x_{mass,in} + \dot{E}x_{sol} = \sum \dot{E}x_D + \dot{E}x_{elect} + \dot{E}x_{mass,out} \tag{35}$$

where $\dot{E}x_D$ and $\dot{E}x_{sol}$ represent the rate of exergy destruction and the rate of input exergy supplied by the sun. The variation in mass flow rate exergy and rate of input exergy from the sun are expressed, respectively, by Equations (36) and (37):

$$\Delta\dot{E}x_{mass} = \dot{E}x_{mass,out} - \dot{E}x_{mass,in} = \dot{m}_f(\psi_{out} - \psi_{in}) \tag{36}$$

$$\dot{E}x_{sol} = \dot{G}\left(1 - \frac{T_0}{T_{sol}}\right) \tag{37}$$

where T_0 and T_{sol} represent the environmental reference temperature and the sun's temperature, respectively.

The overall exergy rate of a PVT collector can therefore be expressed as

$$\dot{E}x_{total} = \dot{E}x_{th} + \dot{E}x_{elect} \tag{38}$$

where the electrical exergy of a PVT collector, $\dot{E}x_{elect}$, equals the rate of electrical energy generated by the solar PVT panels, that is, $\dot{E}_{elect}$ [61].

The exergy efficiencies of a PVT collector consist of both thermal exergy efficiency and electrical exergy efficiency, which are expressed by Equation (39) and Equation (40), respectively, as [56]

$$\eta_{ex,th} = \frac{\dot{E}x_{th}}{\dot{E}x_{sol}} = \frac{\dot{E}x_{mass,out} - \dot{E}x_{mass,in}}{\dot{G}\left(1 - \frac{T_0}{T_{sol}}\right)} \tag{39}$$

$$\eta_{ex,elect} = \frac{\dot{E}x_{elect}}{\dot{E}x_{sol}} = \frac{V_{oc}I_{sc}F}{\dot{G}\left(1 - \frac{T_0}{T_{sol}}\right)} \tag{40}$$

The overall exergy efficiency for a PVT collector is therefore the summation of $\eta_{ex,th}$ and $\eta_{ex,elect}$.

5.3.3. Absorption, DHW, and Cooling Unit

In this section, the exergy balance equations for the components of the absorption chiller, DHW, and cooling units are expressed. The summary of these exergy relations for the proposed hybrid RES components is seen in Table 8.

Table 8. Exergy balances for the various components of the proposed HRES.

Component	Exergy Balance Equation
Pump I	$\dot{E}x_{D,PI} = (\dot{E}x_2 - \dot{E}x_3) + \dot{W}_{PI}$
Pump II	$\dot{E}x_{D,PII} = (\dot{E}x_{11} - \dot{E}x_{12}) + \dot{W}_{PII}$
Pump III	$\dot{E}x_{D,PIII} = (\dot{E}x_8 - \dot{E}x_9) + \dot{W}_{PIII}$
Pump IV	$\dot{E}x_{D,PIV} = (\dot{E}x_{16} - \dot{E}x_{17}) + \dot{W}_{PIV}$
Pump V	$\dot{E}x_{D,PV} = (\dot{E}x_{22} - \dot{E}x_{23}) + \dot{W}_{PV}$
Storage tank	$\dot{E}x_{D,St.Tank} = \dot{E}x_1 + \dot{E}x_5 - \dot{E}x_2 - \dot{E}x_4 - \dot{W}_{St.Tank}$
Absorption chiller	$\dot{E}x_{D,Chill} = (\dot{E}x_7 - \dot{E}x_8) + (\dot{E}x_{10} - \dot{E}x_{11})$
Cooling coil	$\dot{E}x_{D,C.Coil} = (\dot{E}x_9 - \dot{E}x_{10}) + (\dot{E}x_{12} - \dot{E}x_{13})$
DHW tank	$\dot{E}x_{D,Dhw.Tank} = \dot{E}x_{21} + \dot{E}x_{24} - \dot{E}x_{22} - \dot{E}x_{26} - \dot{W}_{Dhw.Tank}$
Flow diverter	$\dot{E}x_{D,Flow.Diverter} = \dot{E}x_{27} - (\dot{E}x_{24} + \dot{E}x_{25})$
Flow mixer I	$\dot{E}x_{D,Flow.MixerI} = \dot{E}x_{25} + \dot{E}x_{28} - Q_{Dhw.out}$
Flow mixer II	$\dot{E}x_{D,Flow.MixerII} = \dot{E}x_{12} + \dot{E}x_{17} - \dot{E}x_{20}$
Flow mixer III	$\dot{E}x_{D,Flow.MixerIII} = \dot{E}x_{20} + \dot{E}x_{23} - \dot{E}x_5$
Heating unit	$\dot{E}x_{D,Heat.unit} = (\dot{E}x_{15} - \dot{E}x_{16}) + (\dot{E}x_{18} - \dot{E}x_{19})$
Diverter valve	$\dot{E}x_{D,Diverter.valve} = \dot{E}x_7 + \dot{E}x_{15} - \dot{E}x_6$

The first law efficiency for the proposed HRES can therefore be defined as follows:

$$\eta_I = \frac{\dot{W}_{net} + \dot{Q}_{cooling} + \dot{Q}_{heating} + \dot{Q}_{Dhw}}{\dot{Q}_{wind,in} + \dot{Q}_{sol}} \tag{41}$$

where $\dot{Q}_{wind,in}$ and $\dot{Q}_{sol}$ is the overall wind energy input and the incident solar radiation, respectively. Additionally, the overall net power ($\dot{W}_{net}$), the cooling capacity ($\dot{Q}_{cooling}$), and the heating capacity ($\dot{Q}_{heating}$) are given as follows:

$$\dot{W}_{net} = \dot{W}_{pvt,total} + \dot{W}_{St.Tank} - \dot{W}_{PI} - \dot{W}_{PII} - \dot{W}_{PIII} - \dot{W}_{PIV} - \dot{W}_{PV} \tag{42}$$

$$\dot{Q}_{cooling} = \dot{m}_{11}(h_{11} - h_{12}) \tag{43}$$

$$\dot{Q}_{heating} = \dot{m}_{18}(h_{18} - h_{19}) \tag{44}$$

Similarly, the second law efficiency for the proposed HRES is expressed as follows:

$$\eta_{II} = \frac{\dot{W}_{net} + \dot{E}x_{cooling} + \dot{E}x_{heating} + \dot{E}x_{Dwh}}{\dot{E}x_{wind,in} + \dot{E}x_{sol}} \tag{45}$$

where $\dot{E}x_{wind,in}$ and $\dot{E}x_{sol}$ represent the overall wind exergy input and the rate of input exergy from the sun, respectively. Additionally, $\dot{E}x_{cooling}$ and $\dot{E}x_{heating}$ can be expressed as

$$\dot{E}x_{cooling} = (\dot{E}x_{13} - \dot{E}x_{14}) \tag{46}$$

$$\dot{E}x_{heating} = (\dot{E}x_{18} - \dot{E}x_{19}) \tag{47}$$

6. Results and Analysis

The analysis of system parameters like temperatures, energy, hot water supply, and a few others, such as the economic metrics of Levelized Cost of Energy (LCOE) and payback period, has been performed for the designed hybrid multigeneration renewable energy system. The dynamic simulation of the system from the TRNSYS environment was run

under the meteorological data of Antalya in the Mediterranean part of Turkey, with the simulation time step set to one hour, and the results were obtained. For easy interpretation of the results, besides the annual graphical representations, monthly and daily representations are also presented where necessary.

6.1. Performance Analysis

Figure 10 shows the annual temperature ranges of the output fluid from the PVT panels. As a result of the solar potential of the location considered (Antalya, Turkey), the PVT is able to supply the needed heat to the fluid. The fluid is heated up to higher temperatures above 90 °C on some days, as can be seen. The PVT working fluid is water, and the occasional outlet temperatures approaching 100 °C under high solar irradiation highlight the importance of adequate circulation in mitigating potential boiling and stagnation risks. Furthermore, elevated operating temperatures may adversely affect PVT electrical efficiency, emphasizing the importance of effective thermal management during system operation. The PVT generates both thermal and electrical energies. The total electrical and thermal energies produced by the HRES for each month are shown in Table 7. The overall electric energy produced is the addition of the electrical energy produced by the PVT and energy produced by the wind turbine.

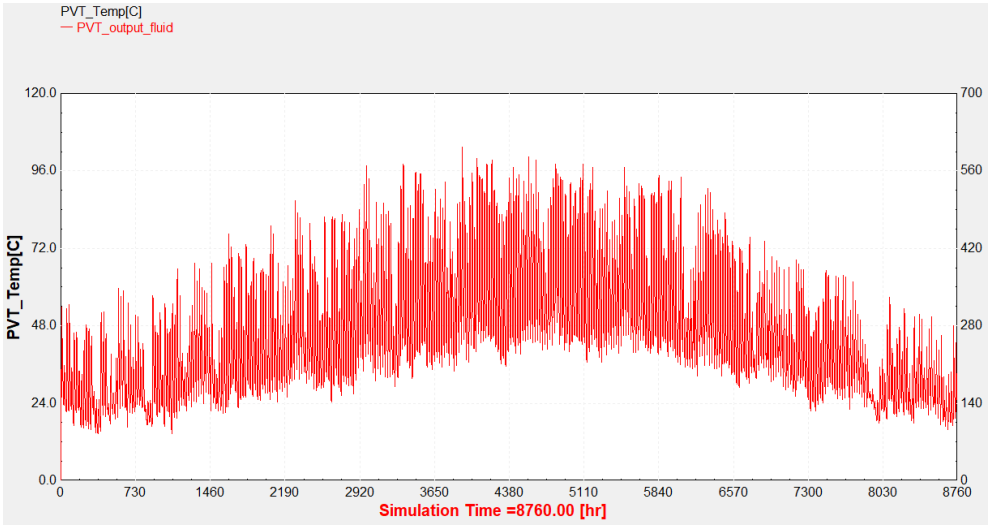


Figure 10. PVT output fluid temperatures for a year.

Figure 11 shows the annual output temperature of the thermal storage tank and the temperature of the DHW outlet. Variation of the averaged temperature is between 45 °C and 95 °C. This variation of the outlet temperature from the storage tank is dependent upon the seasons in the region, with the highest temperatures occurring in the months of June and July. The DHW temperature has been set to maintain a constant temperature of 45 °C by utilizing a configuration that includes flow diverter, flow mixer, and a controller in the DHW production loop. The months with the notable highest daily temperatures and radiation from the sun are the summer months of June, July, and August.

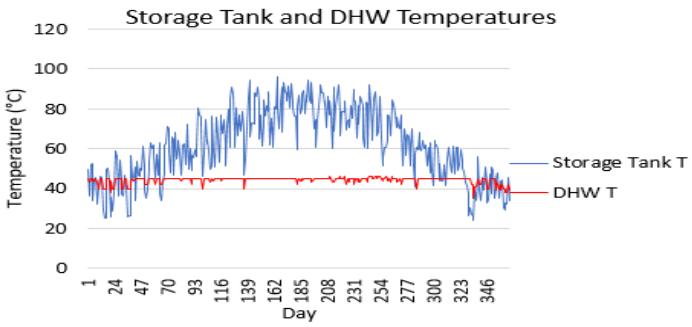


Figure 11. Storage tank and DHW outlet temperatures.

The PVT generates 79.73% of the electricity produced within the system. As seen in Figure 12, the highest electrical generation from the PVT occurs in July (with a value of 299.02 kWh); that is, the month with the highest radiation from the Sun. That goes for the month of January for the wind turbine, with a value of 69.41 kWh. The minimum monthly electrical energy production from both renewable sources occurs in December and August, respectively, with the values of 74.92 kWh and 34.91 kWh, respectively.

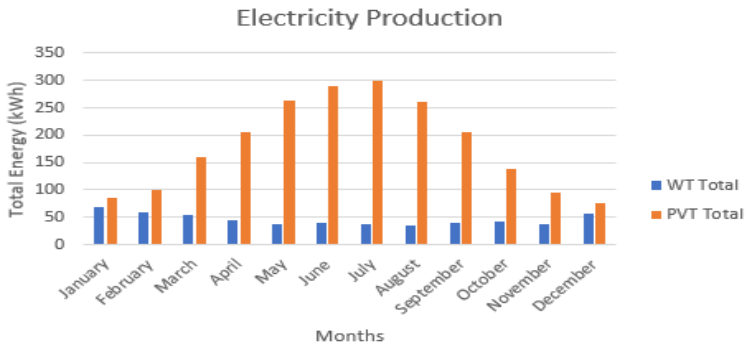


Figure 12. Electrical production by the PVT and wind turbine in different months of the year.

Figure 13 shows the amount of electrical energy generated by the system and the electrical demand for the different months of the year. It reveals that the proposed HRES is able to fully meet the electrical demand of the single-family residential building for the months of April till September; that is, six months. This demonstrates the high solar radiation of Antalya during these months of the year. Surpluses are stored in the electrical battery during the day to be used as the need arises. The minimum total electricity production is recorded for the month of December (at 131.87 kWh).

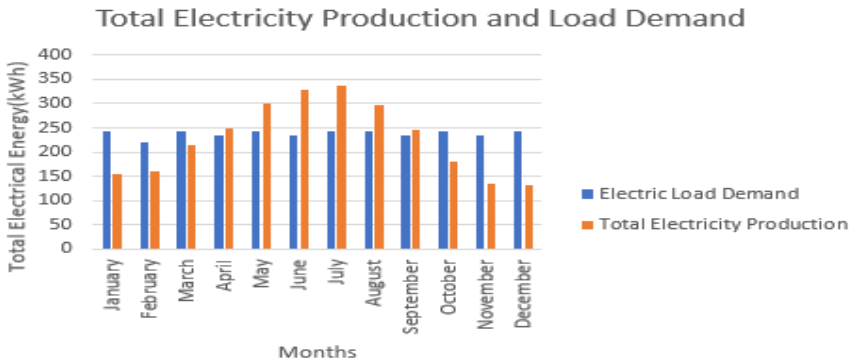


Figure 13. Total electricity generation and electrical load.

The designed hybrid renewable energy multigeneration system from the dynamic TRNSYS environment is also able to give thermal comfort through the production of both cooling energy and space heating by the absorption cooling loop and the space heating loop respectively. These loops are able to supply the space cooling and heating needs of the residential building situated in Antalya, Turkey. The thermal energy required in the system is produced from the PVT modules and it is this energy that supplies the heat required by the absorption chiller for cooling effect, the heating unit for space heating, and the domestic hot water production unit for the supply of hot water for residential use. The thermal energy delivery by the HRES for the different months of the year is shown in Figure 14.

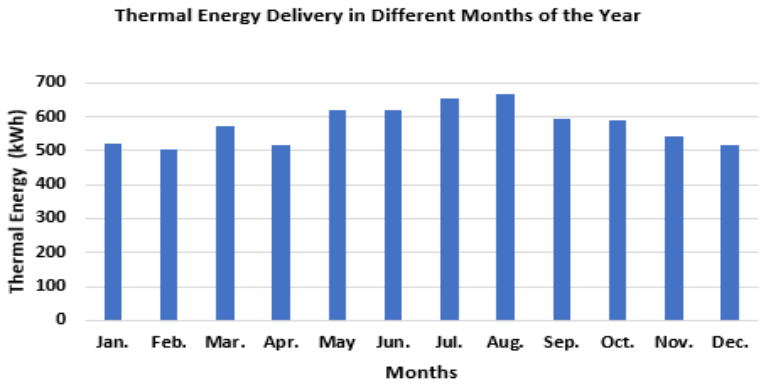


Figure 14. Monthly thermal energy delivered by the PVT.

A yearly thermal energy delivery of 6916.652 kWh is obtained from the proposed hybrid multigeneration system. The cooling demand for the single-family residential building has been presented in Figure 5 above. The system is therefore able to meet the cooling energy requirements of the building for the whole year with an annual production of 3027.083 kWh of cooling energy through the absorption chiller (Figure 15). This production is able to satisfy the 2842.01 kWh annual cooling demands of the building.

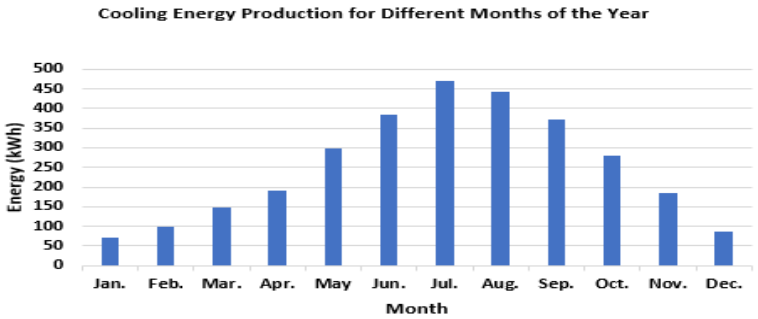


Figure 15. System's cooling production for different months of the year.

Table 9 shows the various energy production and delivery by the HRES over a year period to meet the various energy needs of the residential building.

Table 10 shows the generated electrical and thermal energies by the PVT and WT sources for each of the month in a year.

Considering the electrical energy demand of the residential building, the annual generation by the proposed system is 2730.46 kWh. The energy generated by the system, therefore, lacks 124.84 kWh of electrical energy to completely meet the electrical demand of the residential building. This is in contrast with the cooling energy generation from the absorption cooling loop, which is able to completely satisfy the 2842.01 kWh cooling loads of the residential building. Additionally, the annual thermal energy supplied to the

space-heating unit (179.800 kWh) is able to satisfy the 146.0304 kWh space-heating demand which occurs during the winter months. The measured annual thermal energy delivered to the domestic hot water tap is 2062.710 kWh, while the annual thermal energy supplied to the domestic hot water unit is 2372.117 kWh. The hybrid multigeneration system is therefore able to have a coverage ratio of 95.63% of the building electricity demand, while completely meeting the building's cooling and space heating loads and satisfying the hot water needs of the occupants.

Table 9. Energy production/delivery by the proposed HRES over one year period.

S/N	Parameter	Energy (kWh)	Unit
1	Total electrical energy produced by both PVT and WT	2730.462	kWh
2	Thermal energy delivery by PVT	6916.652	kWh
3	Cooling energy produced from absorption cooling loop	3027.083	kWh
4	Thermal energy delivery to domestic hot water unit	2372.117	kWh
5	Thermal energy delivery to space-heating unit	179.800	kWh

Table 10. Electrical energy and thermal energy produced by both PVT and WT energy sources for each month of the year.

S/N	Month	Total Electrical Energy (kWh)	Thermal Energy (kWh)
1	January	153.62	520.9247
2	February	158.93	504.2251
3	March	215.65	574.3323
4	April	249.13	516.8372
5	May	299.08	620.4044
6	June	329.46	619.8128
7	July	336.74	652.2805
8	August	295.74	665.0184
9	September	245.99	595.6883
10	October	181.02	588.3356
11	November	133.23	541.4742
12	December	131.87	517.3182

Considering the thermal subsystem, the thermal energy from the PVT is delivered to the absorption cooling loop, space-heating loop, and domestic hot water unit. Therefore, the annual thermal energy delivery from the PVT can be expressed as

$$Q_{PVT,th} = Q_{gen,input} + Q_{SH,input} + Q_{DHW,input} + Q_{residual} \quad (48)$$

where $Q_{SH,input}$, $Q_{DHW,input}$, and $Q_{residual}$, represent the thermal energy delivery to space-heating unit, thermal energy delivery to domestic hot water unit, and residual thermal losses. $Q_{gen,input}$ represents the real thermal energy supplied to the absorption chiller, and it is expressed as

$$Q_{gen,input} = \frac{Q_{cool,produced}}{COP} \quad (49)$$

where $Q_{cool,produced}$ is the cooling energy produced from the absorption cooling loop and COP is the absorption chiller's Coefficient of Performance. Therefore,

$$Q_{gen,input} = \frac{3027.083}{0.74} = 4090.653 \text{ kWh/year}$$

Using Equation (12),

$$6916.652 = 4090.653 + 179.800 + 2372.117 + Q_{residual}$$

$Q_{residual}$ = 274.082 kWh/year, which stands for the residual thermal losses or unutilized thermal energy. Table 11 shows the system's thermal energy distribution.

Table 11. Annual thermal energy delivery by the system.

Thermal Branch	Thermal Input (kWh/yr)	Useful Delivery (kWh/yr)
Absorption cooling	$Q_{gen,input}$ = 4090.653	$Q_{cooling}$ = 3027.083
Domestic hot water	$Q_{DHW,input}$ = 2372.117	$Q_{DHW,useful}$ = 2062.710
Space-heating	$Q_{SH,input}$ = 179.800	$Q_{SH,useful}$ = 146.0304

6.2. Parametric Analysis

To assess the influence of key design variables on the performance of the proposed hybrid renewable energy multigeneration system, selected variables of the baseline model were varied independently through a series of TRNSYS simulations. This one-factor-at-a-time parametric analysis was used to identify the parameter values associated with improved system performance within the investigated ranges, particularly increased electricity production while avoiding excessive system sizing. A number of ten different cases are therefore examined, varying the values of four key variables from the base model, which are the total area, inclination angle, and mass flow rate of the solar collector, and the capacity of the main storage tank. Results indicate that increasing the PVT collector area significantly improves electrical energy generation, whereas variations in collector inclination, mass flow rate, and storage volume have negligible effects on electrical output within the investigated ranges. Conversely, reducing the thermal-storage volume generally improves thermal energy delivery, with a particularly pronounced increase for volumes below 5 m^3, suggesting improved thermal utilization and reduced storage-related losses. This can be seen in Table 12 and Figure 16.

Table 12. Annual productions table of the parametric simulations.

S/N	Case Description	Total Electrical Energy (kWh)	Thermal Energy (kWh	Cooling Energy (kWh)
Base Model	Base Design (16 m^2, 45°, 200 kg/h, 2 m^3)	2730.489	6916.652	3027.083
Case I	Tank Volume = 4 m^3	2730.503	6384.760	3011.704
Case II	Tank Volume = 8 m^3	2730.462	5317.925	2096.352
Case III	Tank Volume = 12 m^3	2730.584	5389.627	3002.946
Case IV	Col. Mass Flow Rate = 400 kg/h	2730.489	6916.652	3027.083
Case V	Col. Mass Flow Rate = 1200 kg/h	2730.489	6916.652	3027.083
Case VI	Col. Area = 18 m^2	3002.631	6983.07	3039.535
Case VII	Col. Area = 20 m^2	3274.730	7004.711	3052.044
Case VIII	Col. Slope = 20°	2730.470	6907.636	3024.287
Case IX	Col. Slope = 30°	2730.505	6928.292	3027.339
Case X	Col. Slope = 50°	2730.470	6883.657	3021.142

The collector mass flow rate showed no observable influence on the simulated energy outputs, while variations in collector inclination produced only minor changes. Case VII, corresponding to a 20 m^2 PVT collector area, achieved the highest electrical, thermal, and cooling energy production of 3274.730, 7004.711, and 3052.044 kWh/year, respectively, and was therefore selected as the best-performing configuration among the investigated parametric cases. The configuration presented in Table 13 therefore represents the selected parametric design for the proposed HRES.

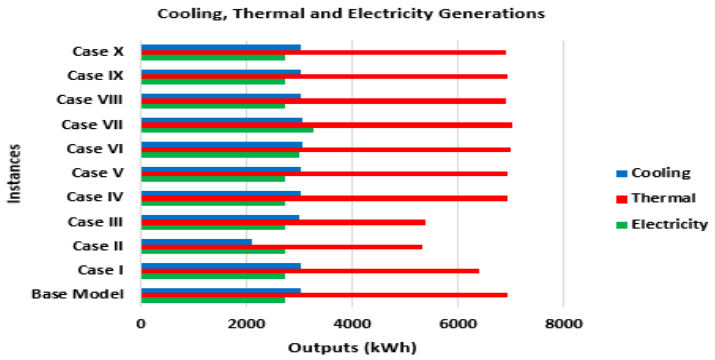


Figure 16. Annual energy productions from the parametric simulations.

Table 13. Best-performing parametric case from the parametric analysis.

Instances	Case Description	Total Electrical Energy (kWh)	Thermal Energy (kWh	Cooling Energy (kWh)
Base Model	Base Design (16 m^2, 45°, 200 kg/h, 2 m^3)	2730.489	6916.652	3027.083
Case VII	Col. Area = 20 m^2	3274.730	7004.711	3052.044

6.3. Validation

Due to the fact that the proposed HRES in its configuration and equipment capacities, as well as the climatic condition considered, has not been reported so far, it is actually impossible to validate the entire work cycle with its different subsystems. The performance of the principal components within the subsystems, which are the PVT and the absorption chiller, was therefore validated against published literature data. For the absorption chiller, the COP of the 11 kW capacity LiBr-H_2O model used in the present study is 0.74 at a generator temperature of 75 °C, compared with the 10 kW residential LiBr-H_2O system reported by Salemeh et al. (2022) [62], which achieved a COP of 0.79 at 100 °C. Both systems were modeled using TRNSYS and serve residential applications, indicating reasonable agreement considering the difference in generator operating temperature. Table 14 shows the result comparison of both studies.

Table 14. Absorption chiller validation with results from Salameh et al. [62].

Parameters	Present Study	Reference Study
Working pair	LiBr_H_2O	LiBr_H_2O
Rated capacity (kW)	11	10 kW house
T_gen (°C)	75	100
COP	0.74	0.79
Application context	Residential	Residential
Modeling platform	TRNSYS	TRNSYS

The PVT model was further compared with the experimental results of Lammle et al. (2018) [63], yielding annual electrical and thermal outputs of 170.65 and 432.29 kWh/(m^2·year), respectively, compared with the reported values of 159 and 445 kWh/(m^2·year) (Table 15). The corresponding deviations of 7.33% for electrical yield and 2.86% for thermal yield indicate reasonable agreement with the experimental reference data, supporting the credibility of the adopted PVT model under the evaluated conditions. However, these component-level comparisons do not constitute comprehensive experimental validation of the integrated HRES.

Table 15. PVT validation with results from Lammle et al. [63].

Parameters	Present Study	Reference Study	Deviation
Electrical yield ($kWh/m^2.yr$)	170.65	159	7.33%
Thermal yield ($kWh/m^2.yr$)	432.29	445	2.86%
Application context	Residential	Residential	-
Modeling platform	TRNSYS	Experimental	-

6.4. Economic Analysis

In order to perform the economic analysis of the proposed HRES in this study, the capital expenditure (which covers the purchase of equipment and installation costs) is first computed. Subsequently, the operational and maintenance expenditure (OPMEX) is obtained as well as other vital economic metrics such as the Net Present Value (NPV), payback period, and Levelized Cost of Energy (LCOE). In this section, it is assumed that all equipment in the system has a lifespan of 20 years with no salvage value. The HRES components and capital expenditures are shown in Table 16.

Table 16. Proposed HRES capital expenditure.

Item No	Item Description	Cost per Unit	No of Units	Cost of Item ($)	Ref.
1	PVT panels (0.275 kWp)	$1500/kWp	11	4537.5	[64]
2	Battery Storage (250 Ah @ 12V)	$300/unit	2	600	[65]
3	Wind Turbine (0.5 kWp)	$3000/kWp	1	1500	[64]
4	Inverter	$1000	1	1000	[64]
5	Absorption Chiller (11 kWp)	$350/kWp	1	3850	[66]
6	Thermal Storage (2 m^3)	$220/$m^3$	1	440	[67]
7	DHW Tank (0.5 m^3)	$220/$m^3$	1	110	[67]
8	Pumps, Valves and Controls	-	-	1650	-
9	Heating Exchanger	$825	1	825	[68]
10	Miscellaneous & Installation	20% total	-	2902.5	-
	Overall CAPEX	**-**	**-**	**17,415**	**-**

In order to obtain the estimate for the OPMEX, the fixed maintenance cost is taken as 4% of CAPEX, which is $696.6 per year. Additionally, the energy cost for pumping and control operation is approximately $200 per year. Battery replacement is assumed to be carried out every 4 years. The initial battery bank costs $600 (two units at $300 each). With a four-year replacement interval and a 20-year project life, the bank is replaced at the end of years 4, 8, 12, and 16. The four replacements cost $2400 in total, giving a simple annual average replacement cost of $120/year ($2400 ÷ 20 years). The annual overall Operation and Maintenance Expenditure for the proposed system is therefore

$$Overall\ annual\ OPMEX = 696.6 + 200 + 120 = \$1016.6$$

The cost assumptions in this study are based on small-scale, commercially available component data rather than large-scale references. Small-scale hybrid renewable energy systems generally exhibit higher specific costs (per kWh or per kW) than large-scale systems due to limited economies of scale. The selection of reference energy systems is dictated by the stand-alone configuration of the proposed hybrid renewable energy system, which is not connected to the electricity grid or natural gas network. Accordingly, diesel-based generation is adopted as the conventional reference for electricity and cooling, representing a diesel generator supplying the cooling unit. For space heating and domestic hot water, LPG-fired boilers and water heaters are used as the reference, consistent with common off-grid heating solutions in remote areas of Turkey where natural gas infrastructure is

absent. Representative unit costs of 0.45 $/kWh for diesel-based electricity and cooling, and 0.14 $/kWh for LPG-based space heating and domestic hot water are assumed based on typical off-grid fuel prices and conversion efficiencies in Turkey. These assumptions ensure that the calculated energy-cost savings correspond to realistic conventional alternatives for stand-alone applications in Antalya, Turkey.

The energy cost savings for the proposed system, with electricity generation of 2730.462 kWh/yr, cooling energy production of 3027.083 kWh/yr, useful space heating delivery of 146.0304 kWh/yr, and domestic hot water production of 2062.710 kWh/year at diesel generator cost of $0.45/kWh and LPG/propane boiler cost of 0.14 kWh/year therefore gives monetary values of $1228.708, $1362.187, and $20.444 kWh/year and $288.779, respectively. This summed up to an overall energy savings value of $2900.12/year.

The Payback Period is calculated from the expression

$$Payback\ Period = \frac{CAPEX}{Savings - OPMEX} \tag{50}$$

The system's Payback Period is therefore estimated as

$$Payback\ Period = \frac{CAPEX}{Savings - OPMEX} = \frac{17,415}{3821.917 - 1134.4} \approx 9.3 \text{ years}$$

In order to find the *NPV* and LCOE estimates for the proposed system, Equations (47) and (50) are utilized.

$$NPV = \sum_{t=1}^{N} \frac{(Energy\ Savings - OPMEX)}{(1 + DR)^t} - CAPEX \tag{51}$$

where N is the system's lifetime assumed as 20 years for this study, and DR is the discount rate taken as 8%, which represents the generally used conventional rate [69]. Therefore,

$$NPV = \sum_{t=1}^{20} \frac{(2900.118 - 1016.6)}{(1 + 0.08)^t} - 17,415$$

$$NPV = +\$1077.66$$

In order to calculate the LCOE, the system's overall useful energy output per year is

$$Total\ useful\ output\ energy/year = 2730.462 + 3027.083 + 146.030 + 2062.710 = 79\ 66.285 \text{ kWh}$$

Unlike conventional electricity-only renewable systems, the proposed hybrid renewable multigeneration system simultaneously delivers four useful energy services, which are electricity, cooling, space heating, and domestic hot water. Accordingly, the *LCOE* is computed using the total annual useful energy delivered by the HRES, which represents the overall cost of supplying integrated energy services rather than only electrical output. Therefore, the *LCOE* is obtained as

$$LCOE = \frac{Total\ Life\ Cycle\ Cost}{Total\ Energy\ Output} \tag{52}$$

$$LCOE = \frac{(17,415 + 20 \times 1016.6)}{20 \times 7966.285} = \$0.237/\text{kWh}$$

The reported *LCOE* therefore represents a system-level useful-energy *LCOE*, an aggregate multigeneration cost metric rather than a conventional electrical *LCOE*. The HRES has demonstrated a strong economic viability. Despite inflationary pressures in Turkey, which also affect the costs of renewable energy components, a drop in costs through the provision of stronger incentives for these renewable energy components by the government will further bring down the initial cost of HRESs, making the system economically attractive.

There already exists a unique renewable energy support mechanism (YEKDEM-2023) in Turkey, which supports increased investments in local manufacturing of renewable energy components, with its attendant benefit of cost reduction [70]. The application of renewable subsidies in diverse forms will encourage the increased utilization of RE, improve Turkey's carbon footprint, and also significantly lower capital expenditure for renewable energy systems in the country.

The utilization of renewable energy systems to meet buildings' energy demands significantly contributes to the avoidance of CO_2, just similar to other sectors. This is achieved by displacing fossil-fuel energy sources such as diesel, liquefied petroleum gas, and natural gas, as well as high-emission grid electricity. Avoiding all these, with their elevated carbon intensity attribute, offers greater environmental benefits. For this study, the avoided operational emissions are calculated using separate conventional reference systems for each energy service and accounting for the corresponding conversion efficiencies. Diesel-based generation was selected as the reference for electricity, while a diesel-fired boiler supplying thermal energy to a single-effect LiBr–H_2O absorption chiller was used as the reference for cooling. LPG-fired systems were selected as the reference for domestic hot water and space heating. The useful cooling energy, $Q_{cool,produced}$ = 3027.083 kWh/year, with the absorption chiller thermal input, Q_{gen} = 3027.083/0.74 = 4090.653 kWh/year. The annual avoided emissions are therefore calculated as

$$M_{CO2,avoided} = \frac{E_{elect}}{\eta_{diesel,gen}} EF_{diesel} + \frac{Q_{gen}}{\eta_{diesel,boiler}} EF_{diesel} + \frac{Q_{DHW}}{\eta_{LPG}} EF_{LPG} + \frac{Q_{SH}}{\eta_{LPG}} EF_{LPG} \quad (53)$$

where $\eta_{diesel,gen}$ = 0.35, $\eta_{diesel,boiler}$ = 0.85, η_{LPG} = 0.90, EF_{diesel} = 0.267 kg CO_2/kWh_{fuel}, and EF_{LPG} = 0.227 kg CO_2/kWh_{fuel} [71,72]. Therefore, using Equation (53), the corresponding annual avoided emissions are 2082.95, 1284.95, 520.26, and 36.83 kg CO_2/year for electricity, cooling, domestic hot water, and space heating, respectively. Thus, the total avoided CO_2 emissions are 3924.99 kg CO_2/year, corresponding to approximately 78,500 kg CO_2, throughout the system's lifespan.

The current environmental assessment focuses on avoided operational emissions, defined as the CO_2 emissions displaced by the useful annual energy delivered to the household by the proposed hybrid renewable energy system, relative to defined conventional reference systems. Embodied emissions associated with the manufacture, transport, installation, maintenance, and end-of-life of system components (e.g., PV modules, batteries, absorption chiller, storage tanks, and piping) are not included in the present analysis. A full life-cycle assessment (LCA) would be required to quantify these additional impacts. The reported value of approximately 3925 kg CO_2/year (which amounts to approximately 78,500 kg CO_2 over 20 years) therefore represents operational-emission avoidance under a full-utilization assumption and should be interpreted as a lower-bound estimate of the system's environmental benefit, since the embodied emissions of the renewable components would partially offset this benefit. In the Mediterranean climate of Antalya, passive night-time cooling can be particularly effective when reduction of daytime cooling loads is concerned. Such demand-side measures would further enhance the net environmental benefit of the proposed system, although their quantification requires a detailed building-level simulation and life-cycle assessment beyond the scope of the present study. Similarly, a conventional alternative such as an air-source heat pump combined with a standard PV array after a low-impact retrofit could achieve comparable or lower total emissions in some scenarios, depending on the specific assumptions regarding system efficiencies, embodied carbon, and grid decarbonization. However, the proposed multigeneration system offers the additional advantage of simultaneously supplying electricity, cooling, domestic hot water, and space heating from a single integrated renewable platform, which may provide operational and resilience benefits not captured by a single-technology comparison.

6.5. System Optimization

The primary goal of system optimization is the enhancement of the proposed HRES while also ensuring cost minimization, zero or reduced dependency on grid power generation, and reduced carbon emissions. The complexity in modeling as well as implementation of HRES integrated with energy storage systems has underscored the significance of inclusion of optimization strategy vital for the optimal sizing of the system's components [73]. This ensures reliable and efficient HRES that are able to sustainably and efficiently meet the intended energy requirements. This study uses Multi-Objective Particle Swarm Optimization (MOPSO) tool as a reliable and flexible technique for optimizing the components of the system. This optimization technique has been employed by several researchers for the provision of reliable solutions to the complex issue of the determination of appropriate size for solar–wind hybrid energy systems, thereby effectively optimizing the capacity of solar panels, wind turbines, and energy storage devices present within the system for optimal performance and output generation [74–77].

Since the optimization technique employed is multi-objective, the primary objective of the optimization is therefore the simultaneous minimization of the system's CAPEX and system-level LCOE with optimal component capabilities while also ensuring the reliability and environmental sustainability of the system. The objective function is therefore expressed as

$$minF(x) = [f_1\ (x), f_2\ (x)] = [CAPEX(x), LCOE(x)] \tag{54}$$

Additionally, the decision vector for the system is expressed as

$$x = (x_{PVT}, x_{WT}, x_{TS}, x_{AC}, x_{HX} x_{Bat}) = [A_{PVT}, P_{WT}, V_{TS}, Q_{AC}, Q_{HX}, C_{Bat}] \tag{55}$$

where $x_{PVT}, x_{WT}, x_{TS}, x_{AC}, x_{HX}, x_{Bat}$ represent the Decision Variables for the PVT, wind turbine, thermal storage tank, absorption chiller, heat exchanger, and battery capacities. Additionally, $A_{PVT}, P_{WT}, V_{TS}, Q_{AC}, Q_{HX}, C_{Bat}$ represent the PVT collector area (m^2), wind turbine rated power (kWp), thermal storage tank volume (m^3), absorption chiller capacity (kW), heat exchanger capacity, and battery storage capacity (kWh), respectively.

For the economic indicators, as seen in the previous section, this study incorporates economic indicators like the CAPEX and OPMEX, Payback Period, NPV and system-level LCOE. This has aided in the effective assessment of the economic viability of the proposed HRES. Annually, the expenditure of the proposed HRES considers: CAPEX, OPMEX, replacement cost, and other system recurring costs. The MOPSO simultaneously minimizes the objective vector in Equation (52). Thus, f_1 (x) minimizes total investment cost, while f_2 (x) minimizes the lifecycle cost of delivered energy. Multi-objective optimization algorithm searches for a set of pareto-optimal solutions. The first objective function minimizes the HRES total installation cost and is expressed in Equation (56) as

$$CAPEX(x) = {}_{C1}\ A_{PVT} + {}_{C2}\ P_{WT} + {}_{C3}\ V_{TS} + {}_{C4}\ Q_{AC} + {}_{C5} Q_{SH} + {}_{C6} C_{Bat} + C_{misc} \tag{56}$$

where *c*1, *c*2, *c*3, *c*4, *c*5, *c*6, and *Cmisc* represent the unit costs of PVT collectors, wind turbine, thermal storage, absorption chiller, space-heating unit, battery storage, and fixed balance of system costs (such as the inverter, piping, controls, and installation). The second objective function minimizes the system's lifecycle energy cost, and the minimized weighted LCOE which employs the electricity energy generation (E), thermal energy production (T) and cooling energy production (C) is expressed as

$$\min WLCOE = \frac{Annualized\ Total\ Cost}{w_e\ .E_{elect} + w_t\ .E_{thermal} + w_c\ .E_{cooling}} \tag{57}$$

where *we*, *wt*, and *wc* represent the normalized weights summing to 1 (for electricity, thermal, and cooling energy respectively, with the thermal energy denoting the combined thermal

flow for space heating and domestic hot water production). Additionally, E_{elec}, $E_{thermal}$, and $E_{cooling}$ are annual useful energy outputs (kWh equivalent). The Annualized Total Cost (ATC) is computed as follows:

$$Annualized\ Total\ Cost\ =\ CRF\ \times \sum_{i}(C_i \times x_i) + O\ \&\ M \tag{58}$$

where C_i is the cost per unit capacity for the energy and storage components, while x_i is the sizing decision variable for component i. *O&M* which is the operating and maintenance costs includes fixed and variable operating & maintenance costs. *CRF* is the capital recovery factor and is given as

$$\mathrm{CRF(i,N)} = \frac{i(i+1)^N}{(i+1)^N - 1} \tag{59}$$

where N is the lifespan of the system which is considered to be 20 years for this study, while i is the annual interest rate taken as 8%. CRF aids in the conversion of the capital cost into annual value that is subsequently employed in the determination of the system-level LCOE. A reduced system-level LCOE means the production of more affordable energy by the proposed hybrid RE system. The MOPSO technique has proven to be beneficial and influential in improving hybrid RE systems and their costs.

The MOPSO optimization for this present study was sequentially coupled with the TRNSYS-based HRES model, with the technical and energy-performance outputs obtained from TRNSYS transferred to the Python optimization framework for techno-economic evaluation. It considered five continuous decision variables: PVT collector area, wind-turbine rated capacity, battery-storage capacity, thermal-storage volume, heating unit capacity, and absorption-chiller capacity. Their respective lower and upper bounds were 6–24 m^2, 0.10–2.00 kW, 2–20 kWh, 0.5–10 m^3, 1–5 kW, and 8–35 kW, with candidate solutions constrained to these ranges during particle updating. The two objectives, CAPEX and system-level LCOE, were treated as equally important independent objectives; hence, no scalar objective-function weighting factors were imposed. The final compromise solution (Point C) was selected from the nondominated Pareto archive after min–max normalization of both objectives using the minimum Euclidean distance from the normalized ideal point.

The Pareto front of the MOPSO is presented in Figure 17. Point C represents the final compromise (optimal) solution. The CAPEX and the system-level LCOE of this knee Point C are 14,618.394 USD and $0.15381/kWh, respectively.

Point A is the case of minimum CAPEX solutions and is characterized by small PVT area, minimal storage and chiller size, and low energy output. Point B is the case of low LCOE solutions, with large PVT area, strong energy outputs, and possible issues of system components oversize. The knee point, which is the optimal solution (point C) satisfies near-minimum CAPEX and near-minimum LCOE objectives, which offer maximum system efficiency per unit cost. Figure 18 depicts the convergence characteristic of the optimization algorithm in minimizing the CAPEX and system-level LCOE of the proposed HRES.

The convergence profiles show a rapid reduction in both the CAPEX and the system-level LCOE during the early iterations, followed by progressively smaller improvements and stabilization. CAPEX converged to approximately USD 13,280, while LCOE stabilized at about USD 0.1412/kWh, with negligible changes thereafter, indicating stable convergence of the MOPSO algorithm within the 200-iteration search horizon. The smooth asymptotic behavior and absence of significant oscillations in the final iterations confirm the good convergence characteristics, stability, and optimization efficiency of the proposed MOPSO algorithm for the HRES design. The optimized design offers a significant increase in the quantity of generated energy from the system in comparison with the baseline scenario. This improvement in the system components' capacity, energy generation, and economic implication is given in Tables 17 and 18 and is in line with the overall objective to achieve

greater system efficiency with optimal performance. It should be noted that although the optimized wind-turbine capacity of 0.101 kW results from treating turbine capacity as a continuous decision variable, practical implementation would require selection of a commercially available turbine with an appropriate rated capacity and reassessment of system performance based on the resulting discrete component specifications.

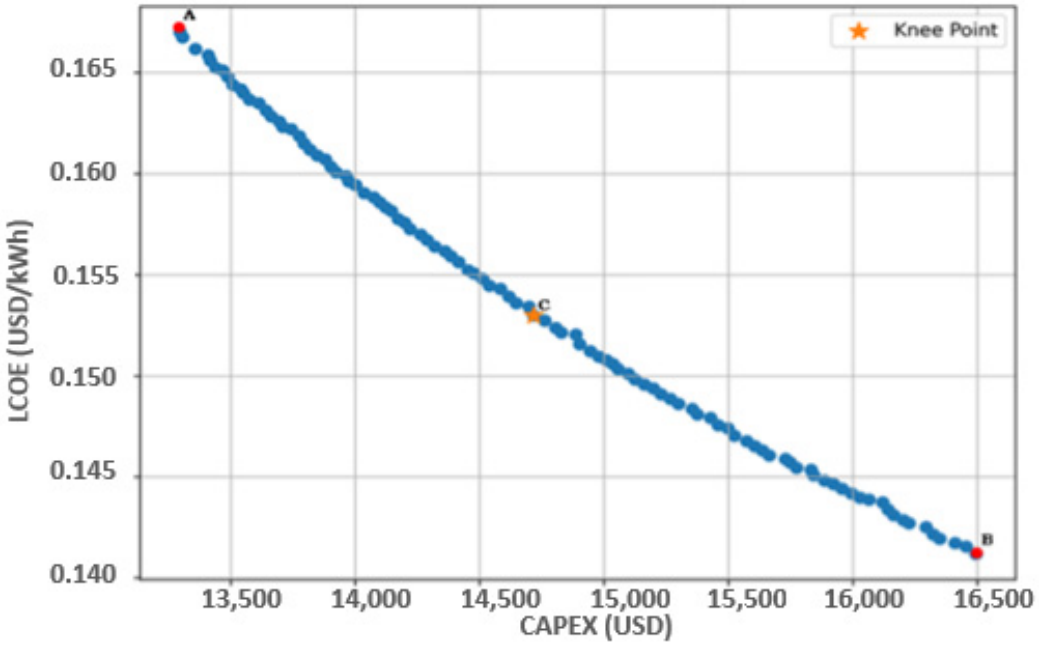


Figure 17. Pareto front.

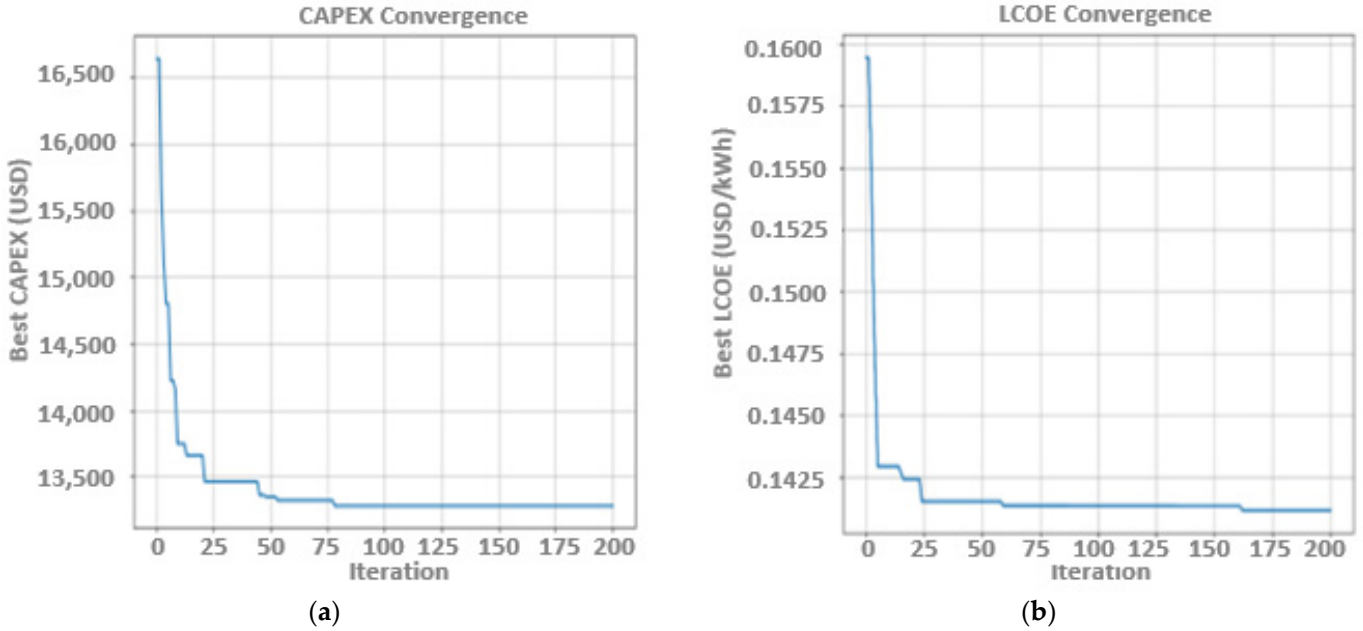


Figure 18. Convergence process of MOPSO algorithm showing how the objective functions evolve over iterations: (**a**) CAPEX convergence; (**b**) LCOE convergence.

From the PSO approach, the load demand has been effectively aligned with the generated renewable energy so that the optimized system is able to fully satisfy the building's load demand, with the generated surplus stored in the storage systems for further usage or sold to the grid in case of on-grid hybrid energy system. The optimized annual electrical energy production of 4773.50 kWh is able to meet the annual load demand of 2855.304 kwh with a surplus. Similarly, the annual thermal production of 7702.85 kWh is able to satisfy the annual baseline thermal energy delivery for the system, while the cooling energy generation of 2847.65 kWh also satisfies the cooling of load 2842.01 kWh. These annual energy outputs from the optimized system are obtained with a significant reduction in both the capital expenditure (CAPEX) and weighted LCOE from $17,415 and $0.237/kWh in the economic analysis section, to $14,618.394 and $0.1538/kWh, respectively. The revised design through the PSO algorithm has therefore led to a 16.1% reduction in the overall capital expenditure (CAPEX) as well as a 35% decrease in the system-level LCOE relative to the modeled baseline. This indicates a more economically efficient energy output system, demonstrating the exceptional merits in the employment of MOPSO algorithm for sizing and optimization of hybrid energy systems.

Table 17. Optimal design components capacities from MOPSO algorithm.

S/N	Component	Optimal Value from MOPSO
1	Wind Turbine Capacity (kWp)	0.101
2	PVT panels (kWp)	4.10
3	Thermal Storage Volume (m^3)	2.019
4	Absorption chiller capacity (kWth)	10.341
5	Heating unit capacity (kWth)	2.00
6	Battery Capacity (kWh)	5.98

Table 18. Final annual energy outputs and costs from MOPSO algorithm.

S/N	Energy/Cost	Optimal Value from MOPSO
1	Annual Electricity output (kWh/year)	4773.10
2	Annual Thermal Energy (kWh/year)	7702.85
3	Annual Cooling Energy (kWh/year)	2847.65
4	Capital Expenditure (CAPEX) (USD)	14,618.394
5	system-level LCOE (USD/kWh)	0.1538

In evaluating the robustness of the MOPSO, the Mean ± Standard Deviation over several independent runs were obtained, as shown in Table 19.

Table 19. Parameter sensitivity analysis for robustness check: Mean ± Standard Deviation Report.

Parameter	CAPEX (Mean ± STD)	LCOE (Mean ± STD)	Runtime (Mean ± STD)	Archive (Mean ± STD)
Swarm Size	14,737.267416 ± 70.860736	0.153062 ± 0.000454	48.271177 ± 32.477185	93.750 ± 37.446543
Iterations	14,733.675578 ± 80.202283	0.152926 ± 0.000541	82.882415 ± 8.400730	99.975 ± 0.158114
Inertia Weight	14,721.362169 ± 71.546610	0.152848 ± 0.000422	73.236035 ± 27.336014	98.850 ± 3.174821
c1	14,731.965252 ± 67.372282	0.152995 ± 0.000524	88.524682 ± 23.909597	97.775 ± 5.071223
c2	14,748.000677 ± 54.561119	0.153034 ± 0.000641	45.560538 ± 34.791970	96.450 ± 7.200249
Archive Size	14,711.398634 ± 55.475431	0.153027 ± 0.000450	85.951836 ± 4.266517	100.000 ± 0.000000
Mutation probability	14,719.097527 ± 57.251549	0.152879 ± 0.000551	43.270823 ± 14.171240	100.000 ± 0.000000

The MOPSO hyperparameter sensitivity was evaluated using a one-factor-at-a-time procedure while retaining the remaining parameters at their baseline values. The investigated ranges were 20–100 particles for swarm size, 50–200 iterations, 0.30–0.90 for inertia weight, 1.0–2.5 for C_1 and C_2, 50–150 for archive size, and 0–0.20 for mutation probability, with 30 independent runs for each setting. The final configuration was 60 particles, 200 iterations, $w = 0.70$, $C_1 = C_2 = 1.50$, archive size = 100, and mutation probability = 0.05. The robustness analysis showed consistently low variability in the CAPEX and the system-level LCOE across the investigated MOPSO parameters, demonstrating strong repeatability and limited sensitivity to stochastic variations. The relatively small standard deviations of the objective values, together with generally stable archive sizes, confirm the robustness and convergence stability of the optimization framework, making it well suited for the multi-objective optimization of the proposed hybrid multigeneration energy system.

To further evaluate the robustness of the proposed hybrid renewable multigeneration system for Antalya, Turkey, uncertainty quantification framework based on Monte Carlo Simulation was performed. The uncertainty assessment employed 1000 Monte Carlo realizations with a fixed random seed of 42. Solar-resource, wind-resource, load-demand, and battery-performance factors were sampled from normal distributions with nominal standard deviations of 10%, 15%, 8%, and 3%, respectively. CAPEX and O&M multipliers followed triangular distributions of (0.90, 1.00, 1.10) and (0.85, 1.00, 1.15), respectively, while the discount rate was sampled uniformly between 6% and 10%. Random inputs were sampled independently with no imposition of prescribed cross-correlations among uncertain input variables. The resulting distributions of CAPEX, system-level LCOE, NPV, and LPSP were subsequently evaluated statistically with Table 20 showing the statistical summary.

Table 20. Uncertainty analysis results.

	LCOE	CAPEX	NPV	LPSP	Load Factor	Solar Factor	Wind Factor	Discount Rate
Mean	0.154625	14,619.962774	3158.194740	0.031531	0.998318	0.995827	1.009194	0.080942
Median	0.153372	14,644.785901	3007.152177	0.002162	0.998880	1.001937	0.998232	0.081848
Std	0.016786	567.232283	694.483608	0.046450	0.059635	0.079335	0.122236	0.011769
Variance	0.000282	321,752.46320	482,307.4824	0.002158	0.003556	0.006294	0.014942	0.000139
Min.	0.110088	13,373.339307	2085.179500	0.00000	0.840439	0.780724	0.736143	0.060724
5%	0.131614	13,675.836319	2298.738730	0.00000	0.896562	0.878093	0.803090	0.063281
50%	0.153372	14,644.785901	3007.152177	0.002162	0.998880	1.001937	0.998232	0.081848
75%	0.163629	14,939.931268	3736.895509	0.050903	1.035696	1.047105	1.078598	0.092448
Max.	0.199869	16,045.496533	4498.884508	0.193000	1.184733	1.175184	1.462328	0.099461

The uncertainty analysis results indicate a mean Loss of Power Supply Probability (LPSP) of 0.0315 (3.15%), demonstrating that the optimized HRES provides a high level of supply reliability under stochastic variations in renewable energy resources and load demand. Figure 19 shows the probability distribution plots of CAPEX, system-level LCOE, NPV, and LPSP.

The probability distributions show that CAPEX and the system-level LCOE are concentrated around their central ranges with moderate dispersion, indicating relatively stable economic performance under the considered uncertainties. NPV remains positive across the simulated realizations, supporting the economic viability of the system under the uncertainty conditions examined. In contrast, the LPSP distribution is strongly right-skewed, with a pronounced concentration near zero and a relatively small number of higher values. Overall, the low mean LPSP and the positively skewed distribution confirm the robustness and resilience of the proposed HRES design for residential energy applications in Antalya, Turkey, while maintaining an acceptable reliability level under uncertainty. The stand-alone system's reliability is influenced by the time-dependent balance between renewable elec-

tricity generation, electrical demand, and battery storage availability. During periods of insufficient solar and wind generation, the battery supplies stored energy to compensate for the generation deficit, subject to its available state of charge (SOC). Unmet electrical demand may occur when renewable generation and the available battery discharge are collectively insufficient to satisfy the load. The Monte Carlo uncertainty analysis accounts for variations in solar and wind availability, electrical demand, and battery performance, yielding a mean LPSP of approximately 3.15%. This value therefore provides an estimated indicator of supply inadequacy under uncertain operating conditions, with resolution of the hourly battery SOC variations not explicitly conducted from the adopted probabilistic formulation.

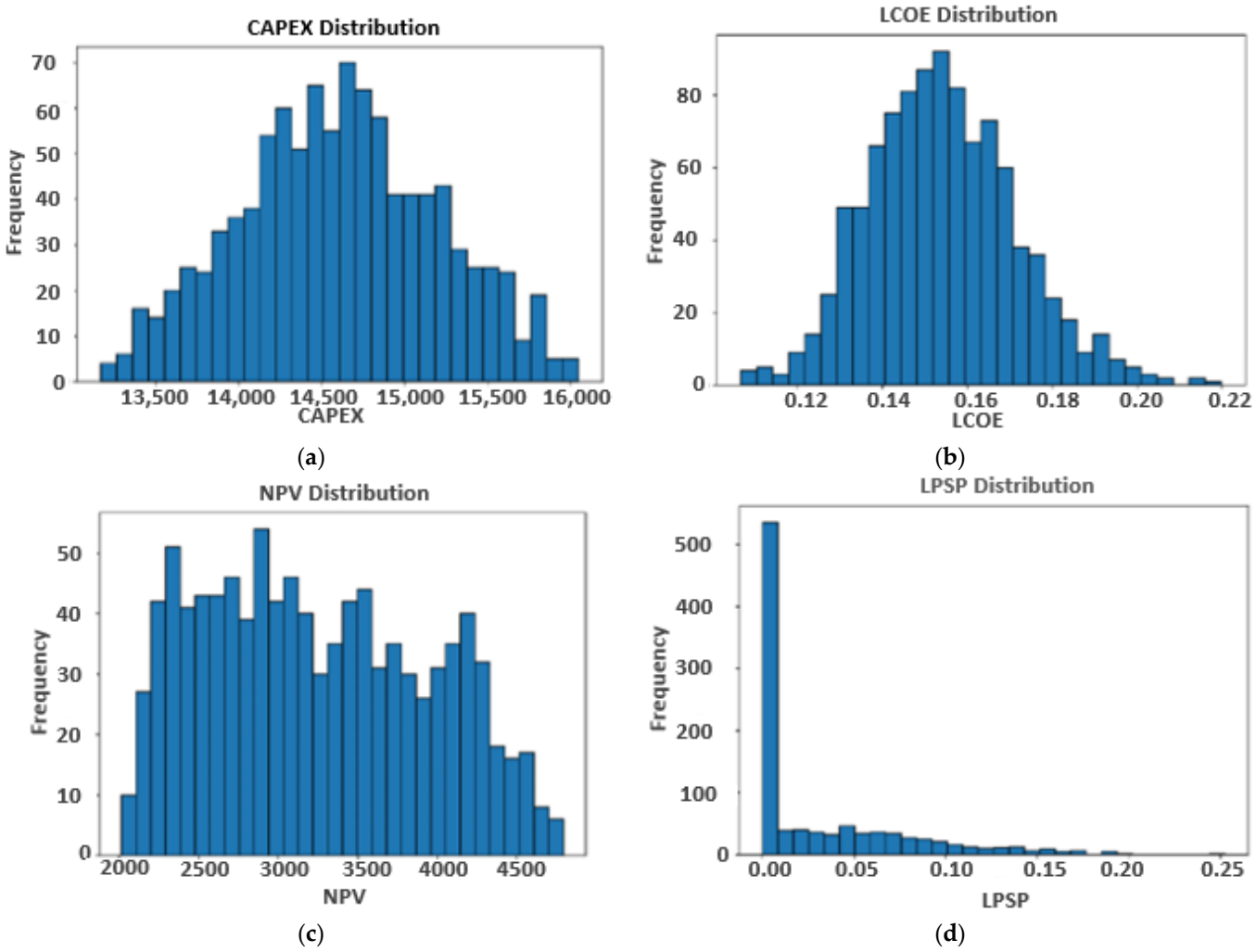


Figure 19. Probability distribution plots: (**a**) CAPEX; (**b**) LCOE; (**c**) NPV; (**d**) LPSP.

Figure 20 shows the correlation matrix derived from the Monte Carlo uncertainty analysis. It reveals the key relationships among the techno-economic and reliability indicators of the proposed HRES. From the matrix, LPSP is positively associated with LCOE ($r = 0.67$) and load factor ($r = 0.57$), while increasing solar and wind availability reduces LPSP ($r = -0.49$ and -0.42, respectively). The strongest relationship is observed between NPV and discount rate ($r = -0.98$), confirming the dominant influence of the discount rate on project profitability. Overall, the correlation analysis confirms that both renewable resource availability and economic parameters are primary drivers of the system's techno-economic performance and reliability under uncertainty.



Figure 20. Correlation heatmap from uncertainty analysis.

7. Practical Implementation Constraints

Although the proposed HRES showed promising performance under the modeled conditions for Antalya, translation of the simulated configuration into a physical residential installation would certainly involve the consideration of potential challenges that include site-specific, operational, reliability, and economic constraints that were not fully represented by the numerical simulation. Site integration and space requirements constitute a crucial implementation constraint. The modeled configuration incorporates a 16 m^2, 3.03 kWp PVT array together with a 0.5 kWp wind turbine and associated thermal-storage and balance-of-system components. Additionally, the optimized system with a 4.1 kWp PVT array requires approximately 22 m^2 of unobstructed collector installation area, alongside adequate space for thermal storage, battery housing, and associated auxiliary equipment. Rooftop geometry, shading, available area, and structural loading constraints are all limitations capable of materially reducing the achievable PVT capacity when considering implementation of multigeneration HRES like the one in this study. The Mediterranean urban setting of Antalya with limited rooftop and yard space, as well as closer neighboring buildings, makes these constraints highly relevant for implementation consideration. The thermal subsystem operation represents another important constraint. This subsystem can present control and temperature challenges during implementation. The absorption chiller requires generator hot water within its specified 75–95 °C operating range, while domestic hot water is supplied at a 45 °C set point. Accordingly, an effective control strategy is required for efficient operation. Additionally, the demand-priority controller distributes available thermal flow between absorption cooling and space heating according to their instantaneous thermal requirements. These requirements increase the importance of appropriate sensor placement, controller tuning, pump operation, and valve response. Failure or calibration drift in these components could therefore reduce useful energy delivery even when sufficient annual renewable energy is theoretically available.

Another practical concern is long-term reliability, since the system contains multiple interacting components that may fail or degrade at different rates. In addition to the PVT modules and wind turbine, the proposed HRES contains an absorption chiller, thermal-storage tanks, battery storage, pumps, heat exchangers, diverter/mixing valves, temperature sensors and control electronics. These interacting components introduce additional potential failure and maintenance points. In particular, pump or sensor failure and valve/controller malfunction can simultaneously affect several downstream energy services. The present simulation does not quantify component failure rates and maintenance intervals; it is important that these are established from manufacturer specifications, as well as field experience before practical deployment. Economic performance is similarly conditional on the assumptions adopted in the study. The calculated CAPEX, system-level LCOE, NPV and payback period depend on the assumed equipment prices, component lifetime, discount rate, electricity valuation and operating/maintenance costs. Changes in local equipment and installation costs, tariffs, financing conditions, exchange rates, and component replacement requirements are all expected to influence actual project economics [78,79]. The economic results therefore present potential viability under the evaluated assumptions rather than the establishment of universal economic feasibility for residential HRES installations in Antalya. In addition, the integration of multiple components (PV modules, battery storage, absorption chiller, thermal storage, and control systems) introduces additional complexity and cost, including the need for advanced control strategies, power electronics, and system-level coordination. These integration efforts can further increase both the capital and operational costs of small-scale systems. Potential incentives or supportive energy policies have the capability of improving investment conditions; however, the present study did not explicitly model any specific government subsidy or financing program and therefore does not quantify their impacts.

Overall, practical deployment of the proposed HRES configuration would require a site-specific engineering assessment incorporating available installation area, structural suitability, hydraulic and control-system integration, reliability requirements, maintenance capability and updated project economics. It is therefore obvious that the actual success of implementing the proposed HRES in a real scenario faces constraints under the modeled Antalya residential conditions, making the present findings offer a basis for further demonstration or pilot-scale assessment.

8. Conclusions

This study developed and dynamically simulated a solar/wind-based hybrid renewable multigeneration system in TRNSYS for supplying electricity, cooling, space heating, and domestic hot water to a single-family residential building in Antalya, Turkey. The analysis comprised the performance evaluation of the baseline configuration, one-factor-at-a-time sensitivity analysis identifying a best-performing parametric configuration (Case VII), economic analysis of the system, multi-objective optimization using MOPSO, and uncertainty analysis of the proposed HRES.

The baseline configuration provided 95.63% annual electrical energy coverage and supplied the modeled thermal-energy services of absorption cooling and space heating, including the prescribed domestic hot water demand of 180 L/day. The parametric analysis showed that the proposed HRES outputs responded differently to changes in the design variables, with variation of the PVT collector area producing the most notable improvement in electricity generation. Case VII was therefore identified as the best-performing configuration among the investigated parametric cases.

The subsequent multi-objective Particle Swarm Optimization analysis constituted the formal optimization stage and identified Pareto-optimal system configurations considering

the selected techno-economic objectives. Relative to the corresponding pre-optimization configuration, the optimization reduced CAPEX and weighted system-level LCOE by 16.1% and 35%, respectively. Furthermore, the uncertainty analysis performed through Monte Carlo simulations produced an LPSP of 3.15%.

Under the economic assumptions adopted in the study, the evaluated HRES produced a positive NPV and a 9.3-year payback period, demonstrating potential economic viability for the investigated residential application. Overall, the results indicate that the proposed multigeneration concept can provide promising techno-economic performance under the Antalya climatic conditions, residential load profiles, component characteristics, control settings, and economic assumptions considered in this study. Future work is expected to expand the framework to other regions and demand profiles in Turkey. Broader geographic comparison of the proposed model would show whether similar multigeneration systems remain attractive across Turkey under different solar, wind, and thermal-load conditions. This would create a stronger basis for policy recommendations and future implementation planning. Additionally, the multi-objective PSO-based sizing optimization can be enhanced through comparison with other metaheuristic algorithm approaches or hybrid AI-based controllers such as neural network assisted PSO.

Author Contributions: Conceptualization, O.D.A. and M.D.; methodology, O.D.A., M.A. (Muhammad Abid) and M.D.; software, O.D.A. and I.D.U.; validation, O.D.A., M.D. and A.M.G.; formal analysis, O.D.A., M.D. and I.D.U.; investigation, O.D.A., M.D. and A.S.; resources, A.S.; data curation, O.D.A.; writing—original draft preparation, O.D.A.; writing—review and editing, O.D.A., M.D., M.A. (Muhammad Abid); visualization, O.D.A.; supervision, M.D., M.A. (Maaz Akhtar) and N.A.A. All authors have read and agreed to the published version of the manuscript.

Funding: This research received no external funding.

Institutional Review Board Statement: Not applicable.

Informed Consent Statement: Not applicable.

Data Availability Statement: The data that support the findings of this study are available from the corresponding author upon reasonable request.

Conflicts of Interest: I.D.U. is an employee of Gordion Beton, Ankara, Turkey. The authors declare no conflicts of interest.

References

1. Petrollese, M.; Cocco, D. Techno-economic assessment of hybrid CSP-biogas power plants. *Renew. Energy* **2020**, *155*, 420–431. [CrossRef]
2. Ayan, O.; Turkay, B.E. Techno-Economic Comparative Analysis of Grid-Connected and Islanded Hybrid Renewable Energy Systems in 7 Climate Regions, Turkey. *IEEE Access* **2023**, *11*, 48797–48825. [CrossRef]
3. Hassan, Q.; Algburi, S.; Sameen, A.Z.; Salman, H.M.; Jaszczur, M. A review of hybrid renewable energy systems: Solar and wind-powered solutions: Challenges, opportunities, and policy implications. *Results Eng.* **2023**, *20*, 101621. [CrossRef]
4. International Energy Agency (IEA). Countries & Regions-Türkiye-Renewables IEA. Available online: https://www.iea.org/countries/turkiye/renewables (accessed on 13 December 2025).
5. Alparslan, U. Türkiye Electricity Review 2025. Available online: https://ember-energy.org/latest-insights/turkiye-electricity-review-2025/ (accessed on 13 December 2025).
6. EMBER. Share of electricity generation in Türkiye. Available online: https://ember-energy.org/data/electricity-data-explorer/?entity=T%C3%BCrkiye&metric=pct_share (accessed on 13 December 2025).
7. European Environment Agency (EEA). *Share of Renewable Energy in Final Energy Consumption*; European Environment Agency (EEA): Copenhagen, Denmark, 2025.
8. Sözen, A.; Arcaklioglu, E.; Özalp, M. Estimation of solar potential in Turkey by artificial neural networks using meteorological and geographical data. *Energy Convers. Manag.* **2004**, *45*, 3033–3052. [CrossRef]

9. Antalya Metropolitan Municipality. Sustainable Energy and Climate Action Plan (SECAP). Available online: https://www.antalya.bel.tr/Content/UserFiles/Files/YarinlardaBizVariz/Dokumanlar/2022/2022-Y%C4%B1l%C4%B1-SECAP.pdf? (accessed on 10 September 2026).
10. Duman, A.C.; Guler, O. Techno-Economic Analysis of Off-Grid PV LED Road Lighting Systems for Antalya Province of Turkey. *Light Eng*. **2019**, *27*, 58–66. [CrossRef]
11. General Directorate of Renewable Energy. Solar Energy Potential Atlas GEPA. Available online: https://enerji.gov.tr/bilgi-merkezi-enerji-gunes-en (accessed on 14 December 2025).
12. Haci, S.; Ismail, B.; Serkan, C. Experimental and numerical analysis of solar potential and feed in tariff in Turkey. In Proceedings of the 2016 IEEE International Conference on Power and Renewable Energy, ICPRE, Shanghai, China, 21–23 October 2016; pp. 594–597. [CrossRef]
13. Arslan, H.; Baltaci, H.; Akkoyunlu, B.O.; Karanfil, S.; Tayanc, M. Wind speed variability and wind power potential over Turkey: Case studies for Çanakkale and İstanbul. *Renew. Energy* **2020**, *145*, 1020–1032. [CrossRef]
14. Elbir, A.; Şahin, M.E. Wind Energy Potential in Turkey's Mediterranean Region: Data Based Analysis and Sustainable Solutions. *Clean Energy Technol*. **2025**, *1*, 1–12. [CrossRef]
15. Togrul, I.T.; Ertekin, C. A statistical investigation on the wind energy potential of Turkey's geographical regions. *Energy Sources Part A Recovery Util. Environ. Eff*. **2011**, *33*, 1399–1421. [CrossRef]
16. Alhijazi, A.A.K.; Almasri, R.A.; Alloush, A.F. A Hybrid Renewable Energy (Solar/Wind/Biomass) and Multi-Use System Principles, Types, and Applications: A Review. *Sustainability* **2023**, *15*, 16803. [CrossRef]
17. El-Sattar, H.A.; Kamel, S.; Sultan, H.M.; Zawbaa, H.M.; Jurado, F. Optimal design of Photovoltaic, Biomass, Fuel Cell, Hydrogen Tank units and Electrolyzer hybrid system for a remote area in Egypt. *Energy Rep*. **2022**, *8*, 9506–9527. [CrossRef]
18. Godiño, J.A.V.; García, M.T. Techno-Economic Assessment of an Innovative Small-Scale Solar-Biomass Hybrid Power Plant. *Appl. Sci*. **2023**, *13*, 8179. [CrossRef]
19. Bhatti, U.; Aamir, H.; Kamal, K.; Ratlamwala, T.A.H.; Alqahtani, F.; Alkahtani, M.; Mohammad, E.; Alatefi, M. Clean Energy Based Multigeneration System for Sustainable Cities: Thermodynamic, and Stability Analyses. *Membranes* **2023**, *13*, 358. [CrossRef]
20. Gómez, L.; León Aldaco, D.; Alquicira, A.; León Gómez, J.C.; De León Aldaco, S.E.; Aguayo Alquicira, J. A Review of Hybrid Renewable Energy Systems: Architectures, Battery Systems, and Optimization Techniques. *Eng* **2023**, *4*, 1446–1467. [CrossRef]
21. Afrouzi, H.N.; Hassan, A.; Wimalaratna, Y.P.; Ahmed, J.; Mehranzamir, K.; Liew, S.C.; Malek, Z.A. Sizing and economic analysis of stand-alone hybrid photovoltaic-wind system for rural electrification: A case study Lundu, Sarawak. *Clean. Eng. Technol*. **2021**, *4*, 100191. [CrossRef]
22. Allouhi, H.; Allouhi, A.; Almohammadi, K.M.; Hamrani, A.; Jamil, A. Hybrid renewable energy system for sustainable residential buildings based on Solar Dish Stirling and wind Turbine with hydrogen production. *Energy Convers. Manag*. **2022**, *270*, 116261. [CrossRef]
23. Babalola, K.Z.; Elenga, R.G.; Mushtaque, A.; Genovese, P.V.; Aborisade, M.A. Hybrid Optimisation of PV/Wind/BS Standalone System for Sustainable Energy Transition: Case Study of Nigeria. *Energies* **2026**, *19*, 89. [CrossRef]
24. Savio, F.M.; Joshua, S.V.; Usha, K.; Faheem, M.; Kannadasan, R.; Khan, A.A. Design of a Solar-Wind Hybrid Renewable Energy System for Power Quality Enhancement: A Case Study of 2.5 MW Real Time Domestic Grid. *Eng. Rep*. **2025**, *7*, e13101. [CrossRef]
25. Charles Rajesh Kumar, J.; Majid, M.A. Advances and development of wind–solar hybrid renewable energy technologies for energy transition and sustainable future in India. *Energy Environ*. **2024**, *35*, 2517–2565. [CrossRef]
26. He, M.; Fard, H.F.; Yahya, K.; Mohamed, M.; Alhamrouni, I.; Awalin, L.J. Optimal Design of Hybrid Renewable Systems, Including Grid, PV, Bio Generator, Diesel Generator, and Battery. *Sustainability* **2023**, *15*, 3297. [CrossRef]
27. Lata-García, J.; Cedeño, N.Z.; Ampuño, G.; Jurado, F.; Swarupa, M.L.; Maliza, W. Optimization and Evaluation of a Stand-Alone Hybrid System Consisting of Solar Panels, Biomass, Diesel Generator, and Battery Bank for Rural Communities. *Sustainability* **2024**, *16*, 9012. [CrossRef]
28. Ganjei, N.; Zishan, F.; Alayi, R.; Samadi, H.; Jahangiri, M.; Kumar, R.; Mohammadian, A. Designing and Sensitivity Analysis of an Off-Grid Hybrid Wind-Solar Power Plant with Diesel Generator and Battery Backup for the Rural Area in Iran. *J. Eng*. **2022**, *2022*, 4966761. [CrossRef]
29. Oymak, A.; Tur, M.R. Decarbonizing Rural Off-Grid Areas Through Hybrid Renewable Hydrogen Systems: A Case Study from Turkey. *Processes* **2025**, *13*, 2909. [CrossRef]
30. Alshammari, S.; Fathy, A. Optimum Size of Hybrid Renewable Energy System to Supply the Electrical Loads of the Northeastern Sector in the Kingdom of Saudi Arabia. *Sustainability* **2022**, *14*, 13274. [CrossRef]
31. Mahmoud, F.S.; Diab, A.A.Z.; Ali, Z.M.; El-Sayed, A.-H.; Alquthami, T.; Ahmed, M. Optimal sizing of smart hybrid renewable energy system using different optimization algorithms. *Energy Rep*. **2022**, *8*, 4935–4956. [CrossRef]
32. Alzaid, O.S.; Salim, B.; Orfi, J.; Khan, S.; Alshehri, H. Hybrid Solar and Wind Power Generation in Saudi Arabia. *Energy Environ. Res*. **2020**, *10*, 25. Available online: https://EconPapers.repec.org/RePEc:ibn:eerjnl:v:10:y:2022:i:2:p:25 (accessed on 10 October 2026).

33. Bozkurt, A.; Genc, M.S.; Seyitoglu, S.S. 7E analysis of a low-temperature geothermal and solar energy integrated hybrid system for sustainable power and hydrogen generation. *Therm. Sci. Eng. Prog.* **2025**, *66*, 104073. [CrossRef]
34. Muleta, N.; Badar, A.Q.H. Designing of an optimal standalone hybrid renewable energy micro-grid model through different algorithms. *J. Eng. Res.* **2023**, *11*, 100011. [CrossRef]
35. Pürlü, M.; Andiç, C.; Aydın, E.; Solak, B. Optimal Design of Hybrid Renewable Energy System for a Region in Turkey Using HOMER. *Turk. J. Electr. Power Energy Syst.* **2023**, *3*, 146–155. [CrossRef]
36. Turkish Standard Institute. *TS 825-Thermal Insulation Requirements for Buildings*; Turkish Standard Institute: Ankara, Turkey, 2008.
37. Meteonorm 8. Available online: https://meteonorm.com/ (accessed on 12 September 2021).
38. Issi, F.; Kaplan, O. The Determination of Load Profiles and Power Consumptions of Home Appliances. *Energies* **2018**, *11*, 607. [CrossRef]
39. Aplas Group Solar Energy. Antalya Gün Işı Rehberi. Available online: https://www.aplasgroup.com.tr/antalya-gun-isi-fiyatlari-2026-aplas/ (accessed on 23 September 2026).
40. Ileri, A.; Moshiri, S. Effects of common fuel and heating system options on the energy usage, pollutant emissions and economy. *Energy Build.* **1996**, *24*, 11–18. [CrossRef]
41. ENF Solar. Wiosun CM Series PERC 275-285M Solar Panel Datasheet. Available online: https://www.enfsolar.com/pv/panel-datasheet/crystalline/33743 (accessed on 24 October 2025).
42. A-Wing International. YWS-500 Micro Wind Turbine. Available online: http://www.awing-i.com/english/E500T.pdf (accessed on 19 July 2026).
43. Thomson, M. CREST Domestic Electricity Demand Model. Available online: https://repository.lboro.ac.uk/articles/dataset/Domestic_electricity_demand_model_-_simulation_example/9512927?file=17140067 (accessed on 12 August 2025).
44. Florides, G.A.; Kalogirou, S.A.; Tassou, S.A.; Wrobel, L.C. Modelling, simulation and warming impact assessment of a domestic-size absorption solar cooling system. *Appl. Therm. Eng.* **2002**, *22*, 1313–1325. [CrossRef]
45. Khanmohammdi, S.; Musharavati, F.; Sheykhmohammadi, M. Energy and exergy examinations of a PVT based hybrid system for power, heating and potable water production: Transient modeling. *Renew. Energy* **2022**, *195*, 540–553. [CrossRef]
46. Rejeb, O.; Dhaou, H.; Jemni, A. Parameters effect analysis of a photovoltaic thermal collector: Case study for climatic conditions of Monastir, Tunisia. *Energy Convers. Manag.* **2015**, *89*, 409–419. [CrossRef]
47. Khanmohammadi, S.; Abdi Chaghakaboodi, H.; Musharavati, F. Solar-based Kalina cycle integrated with PEM fuel cell boosted by thermoelectric generator: Development and thermodynamic analysis. *Int. J. Green Energy* **2021**, *18*, 866–878. [CrossRef]
48. Tahir, M.F.; Haoyong, C.; Guangze, H.; Mehmood, K. Energy and exergy analysis of wind power plant: A case study of Gharo, Pakistan. *Front. Energy Res.* **2022**, *10*, 1008989. [CrossRef]
49. Mehrpooya, M.; Moftakhari Sharifzadeh, M.M.; Rosen, M.A. Energy and exergy analyses of a novel power cycle using the cold of LNG (liquefied natural gas) and low-temperature solar energy. *Energy* **2016**, *95*, 324–345. [CrossRef]
50. Sahin, A.D.; Dincer, I.; Rosen, M.A. New Spatio-Temporal Wind Exergy Maps. *J. Energy Resour. Technol.* **2006**, *128*, 194–201. [CrossRef]
51. Patel, M.R.; Beik, O. *Wind and Solar Power Systems: Design, Analysis, and Operation*, 3rd ed.; CRC Press: Boca Raton, FL, USA, 2021. [CrossRef]
52. Dincer, I.; Rosen, M.A. Exergy Analysis of Renewable Energy Systems. In *Exergy: Energy, Environment and Sustainable Development*, 1st ed.; Elsevier Ltd.: Amsterdam, The Netherlands, 2007; Chapter 10.
53. Lanchester, F.W. A Contribution to the Theory of Propulsion and the Screw Propeller. *J. Am. Soc. Nav. Eng.* **1915**, *27*, 509–510. [CrossRef]
54. Redha, A.M.; Dincer, I.; Gadalla, M. Thermodynamic performance assessment of wind energy systems: An application. *Energy* **2011**, *36*, 4002–4010. [CrossRef]
55. Khanjari, A.; Mahmoodi, E.; Ahmadi, M.H. Energy and exergy analyzing of a wind turbine in free stream and wind tunnel in CFD domain based on actuator disc technique. *Renew. Energy* **2020**, *160*, 231–249. [CrossRef]
56. Kazemian, A.; Taheri, A.; Sardarabadi, A.; Ma, T.; Passandideh-Fard, M.; Peng, J. Energy, exergy and environmental analysis of glazed and unglazed PVT system integrated with phase change material: An experimental approach. *Sol. Energy* **2020**, *201*, 178–189. [CrossRef]
57. Bejan, A.; Tsatsaronis, G.; Moran, M.J. *Thermal Design and Optimization*; John Wiley & Sons: New York, NY, USA, 1995.
58. Hepbasli, A.; Alsuhaibani, Z. Exergetic and exergoeconomic aspects of wind energy systems in achieving sustainable development. *Renew. Sustain. Energy Rev.* **2011**, *15*, 2810–2825. [CrossRef]
59. Khanmohammadi, S.; Musharavati, F.; Tariq, R. A framework of data modeling and artificial intelligence for environmental-friendly energy system: Application of Kalina cycle improved with fuel cell and thermoelectric module. *Process Saf. Environ. Prot.* **2022**, *164*, 499–516. [CrossRef]

60. Sardarabadi, M.; Hosseinzadeh, M.; Kazemian, A.; Passandideh-Fard, M. Experimental investigation of the effects of using metal-oxides/water nanofluids on a photovoltaic thermal system (PVT) from energy and exergy viewpoints. *Energy* **2017**, *138*, 682–695. [CrossRef]
61. Çiftçi, E.; Khanlari, A.; Sözen, A.; Aytaç, İ.; Tuncer, A.D. Energy and exergy analysis of a photovoltaic thermal (PVT) system used in solar dryer: A numerical and experimental investigation. *Renew. Energy* **2021**, *180*, 410–423. [CrossRef]
62. Salameh, T.; Alkhalidi, A.; Rabaia, M.K.H.; Al Swailmeen, Y.; Alroujmah, W.; Ibrahim, M.; Abdelkareem, M.A. Optimization and life cycle analysis of solar-powered absorption chiller designed for a small house in the United Arab Emirates using evacuated tube technology. *Renew. Energy* **2022**, *198*, 200–212. [CrossRef]
63. Lämmle, M.; Hermann, M.; Kramer, K.; Panzer, C.; Piekarczyk, A.; Thoma, C.; Fahr, S. Development of highly efficient, glazed PVT collectors with overheating protection to increase reliability and enhance energy yields. *Sol. Energy* **2018**, *176*, 87–97. [CrossRef]
64. Kilic, M.; Altun, A.F. Dynamic modelling and multi-objective optimization of off-grid hybrid energy systems by using battery or hydrogen storage for different climates. *Int. J. Hydrogen Energy* **2023**, *48*, 22834–22854. [CrossRef]
65. Ijeoma, M.W.; Chen, H.; Carbajales-Dale, M.; Yakubu, R.O. Techno-Economic Assessment of the Viability of Commercial Solar PV System in Port Harcourt, Rivers State, Nigeria. *Energies* **2023**, *16*, 6803. [CrossRef]
66. Roncal-Casano, J.J.; Taddeo, P.; Rodriguez-Martin, J.; Munoz-Anton, J.; Velasco, A.A. Techno-economic comparison of a solar absorption chiller and photovoltaic compression chiller. In Proceedings of the ECOS 2023—The 36th International Conference on Efficiency, Cost, Optimization, Simulation and Environmental Impact of Energy Systems, Las Palmas De Gran Canaria, Spain, 25–30 June 2023.
67. Lüchinger, R.; Hendry, R.; Walter, H.; Worlitschek, J.; Schuetz, P. Cost Analysis for Large Thermal Energy Storage Systems. *J. Eng. Sustain. Build. Cities* **2025**, *6*, 021006. [CrossRef]
68. Kalyan, M.; Pulagam, R.; Kumar Rout, S.; Sarangi, S.K. A state-of-the-art review on thermo fluid performance of brazed plate heat exchanger for HVAC application. *J. Therm. Eng.* **2024**, *10*, 1390–1410. [CrossRef]
69. Kpalo, S.Y.; Zainuddin, M.F.; Manaf, L.A.; Roslan, A.M.; Nik Ab Rahim, N.N.R. Techno-Economic Viability Assessment of a Household Scale Agricultural Residue Composite Briquette Project for Rural Communities in Nigeria. *Sustainability* **2022**, *14*, 9399. [CrossRef]
70. Erdem, M.; Gürtürk, M. Economic analysis of the impact of Turkey's renewable support mechanism on solar energy investment. *Util. Policy* **2025**, *92*, 101862. [CrossRef]
71. IPCC. 2006 IPCC Guidelines for National Greenhouse Gas Inventories. Volume 2: Energy. Available online: https://www.ipcc-nggip.iges.or.jp/public/2006gl/pdf/2_Volume2/V2_1_Ch1_Introduction.pdf (accessed on 14 September 2026).
72. Flammini, A.; Pan, X.; Tubiello, F.N.; Qiu, S.Y.; Souza, L.R.; Quadrelli, R.; Bracco, S.; Benoit, P.; Sims, R. Emissions of greenhouse gases from energy use in agriculture, forestry and fisheries: 1970–2019. *Earth Syst. Sci. Data* **2022**, *14*, 811–821. [CrossRef]
73. Bamisile, O.; Cai, D.; Adun, H.; Dagbasi, M.; Ukwuoma, C.C.; Huang, Q.; Johnson, N.; Bamisile, O. Towards Renewables Development: Review of Optimization Techniques for Energy Storage and Hybrid Renewable Energy Systems. *Heliyon* **2024**, *10*, e37482. [CrossRef]
74. Bade, S.O.; Tomomewo, O.S.; Meenakshisundaram, A.; Dey, M.; Alamooti, M.; Halwany, N. Multi-Criteria Optimization of a Hybrid Renewable Energy System Using Particle Swarm Optimization for Optimal Sizing and Performance Evaluation. *Clean Technol.* **2025**, *7*, 23. [CrossRef]
75. HassanzadehFard, H.; Tooryan, F.; Collins, E.R.; Jin, S.; Ramezani, B. Design and optimum energy management of a hybrid renewable energy system based on efficient various hydrogen production. *Int. J. Hydrogen Energy* **2020**, *45*, 30113–30128. [CrossRef]
76. Sharafi, M.; ELMekkawy, T.Y. Multi-objective optimal design of hybrid renewable energy systems using PSO-simulation based approach. *Renew. Energy* **2014**, *68*, 67–79. [CrossRef]
77. Shahid, Z.; Santarelli, M.; Marocco, P.; Ferrero, D.; Zahid, U. Techno-economic feasibility analysis of Renewable-fed Power-to-Power (P2P) systems for small French islands. *Energy Convers. Manag.* **2022**, *255*, 115368. [CrossRef]
78. Ağbulut, Ü.; Yıldız, G.; Bakır, H.; Polat, F.; Biçen, Y.; Ergün, A.; Gürel, A.E. Current practices, potentials, challenges, future opportunities, environmental and economic assumptions for Türkiye's clean and sustainable energy policy: A comprehensive assessment. *Sustain. Energy Technol. Assess.* **2023**, *56*, 103019. [CrossRef]
79. Dindar, S. A Comprehensive Analysis of Strategies, Challenges and Policies on Turkish Sustainable Energy Development. *J. Eng. Technol. Appl. Sci.* **2022**, *7*, 231–250. [CrossRef]

Disclaimer/Publisher's Note: The statements, opinions and data contained in all publications are solely those of the individual author(s) and contributor(s) and not of MDPI and/or the editor(s). MDPI and/or the editor(s) disclaim responsibility for any injury to people or property resulting from any ideas, methods, instructions or products referred to in the content.